

# Evolution of Linear Perturbations under Time-Dependent Hubble Friction I: SR-USR-SR Inflation

Wen Li,<sup>1</sup> Chao Chen<sup>1,\*</sup>

<sup>1</sup> School of Science, Jiangsu University of Science and Technology, Zhenjiang, 212100, China

## Abstract

In this paper, we revisit the linear perturbation (including the comoving curvature perturbation and field perturbation) dynamics in the SR–USR–SR inflation with instantaneous transitions. Using the junction method and asymptotic expansions of Hankel functions, we derive accurate asymptotic expressions for the time evolution of mode functions and the resulting power spectrum, based on three systematic rules for identifying the dominant terms across transitions. Our results reveal that a finite dip of the final power spectrum arises from the cancellation between two growing modes within the linear perturbation theory, rather than between constant and growing terms as previously suggested. We also provide analytical descriptions of the amplitude enhancement and oscillatory features in the linear power spectrum, in agreement with numerical computations. These simple, tractable formulas not only facilitate theoretical calculations but also yield testable predictions for future CMB observations.

## Contents

<b>1</b>	<b>Introduction</b>	<b>2</b>
<b>2</b>	<b>Analytic Solutions from the Junction Method</b>	<b>4</b>
2.1	General solutions . . . . .	4
2.2	Junction method: SR-USR-SR . . . . .	4
2.3	Asymptotics on superhorizon scales: finite growing modes . . . . .	6
2.4	Asymptotics on subhorizon scales . . . . .	8
<b>3</b>	<b>Time Evolutions of Power Spectra</b>	<b>10</b>
3.1	Case 1 . . . . .	10
3.1.1	USR . . . . .	10
3.1.2	SR2 . . . . .	12
3.1.3	The dip structure of the final power spectrum . . . . .	16
3.2	Case 3 . . . . .	18
3.3	Case 2 . . . . .	21

\*Corresponding author: cchao012@just.edu.cn;

<b>4 Conclusion</b>	<b>24</b>
<b>A Consistent Check</b>	<b>24</b>

# 1 Introduction

The slow-roll (SR) inflation, the simplest and most popular inflationary scenario, naturally explains the nearly scale-invariant power spectrum of primordial curvature perturbations observed on large scales in the cosmic microwave background radiation (CMB) [1]. However, the statistics of primordial curvature perturbations on small scales remain poorly constrained (c.f., Fig. 14 in Ref. [2] or Fig. 1 in Ref. [3]), primarily due to the challenges of highly nonlinear evolutions and the limited sensitivity of current experiments. This leaves significant scope for theoretical models beyond the vanilla slow-roll scenario, particularly those that predict a strong enhancement of small-scale curvature perturbations. In this context, the ultra-slow-roll (USR) inflation stands as the most prominent scenario, enabling such an enhancement that leads to rich phenomena, including primordial black hole (PBH) formation and scalar-induced gravitational waves (e.g., see reviews [2, 4–7] for more details). The USR inflation offers not only rich phenomenology but also compelling theoretical motivations: it serves as a simple model for analyzing non-perturbative effects on primordial curvature perturbation statistics [8–32], while the quantum one-loop corrections induced by enhanced small-scale perturbations during this phase remain an open and intriguing topic [33–63].

The simplest USR model exhibits a sandwich structure: where the USR phase serves as an intermediate stage between two SR phases, as illustrated in the left panel of Fig. 1. Throughout this paper, the USR phase is defined by the second slow-roll parameter,  $\eta \equiv \dot{\epsilon}/(\epsilon H) = -6$ ,<sup>1</sup> where  $\epsilon \equiv -\dot{H}/H^2$  is the slow-roll parameter and the dot refers to the time derivative. The USR inflation can be classified within a broader concept of constant-roll (CR) inflation, where  $\eta$  is a constant [70]. During the USR phase, the inflationary potential becomes nearly flat, and the inflaton’s motion is dominated by Hubble friction rather than the potential gradient. This makes the USR phase a non-attractor regime, where perturbations exhibit distinct behaviors compared with that of SR phase. In particular, the linear comoving curvature perturbation  $\mathcal{R}$  develops a growing mode on superhorizon scales during USR [71, 73–78], which ultimately enhances the curvature power spectrum  $\mathcal{P}_{\mathcal{R}}(k) \equiv \frac{k^3}{2\pi^2} |\mathcal{R}_k(\tau_{\text{end}})|^2$  at the end of inflation  $\tau_{\text{end}} \rightarrow 0^-$ .<sup>2</sup> This enhancement can be understood intuitively from the linear equation of motion (EoM) for  $\mathcal{R}_k$ ,

$$\ddot{\mathcal{R}}_k + (3 + \eta)H\dot{\mathcal{R}}_k + \frac{k^2}{a^2}\mathcal{R}_k = 0, \quad (1)$$

where a growing mode emerges in the solution, once the effective Hubble friction coefficient  $(3 + \eta)H$  becomes negative (i.e., when  $\eta < -3$ ) [71, 73]. Utilizing the junction method, Ref. [73] first identified the steepest possible  $k^4$  growth in the linear power spectrum  $\mathcal{P}_{\mathcal{R}}(k)$  in USR inflation. Later work [74] showed that an even steeper scaling,  $k^5(\ln k)^2$ , can arise if a CR phase with  $\eta = -1$  is incorporated. This work also employed the perturbative method to analyze the dip structure observed

<sup>1</sup>In literature, the definition of the USR phase varies. For instance, Refs. [64–66] characterize it by a flat potential, i.e.,  $V_{,\phi} \equiv dV/d\phi = 0$ , while Refs. [9, 67–70] define USR as a regime where  $\beta \equiv \ddot{\phi}/(H\dot{\phi}) = -3$ . In this work, we adopt the definition used in Refs. [71, 72], which aligns with other conventions through the relation  $\eta = -6 - 2\frac{V_{,\phi}}{H\dot{\phi}} + 2\epsilon = 2\beta + 2\epsilon$ .

<sup>2</sup>Here, the superscript “-” of 0 means that  $\tau_{\text{end}}$  approaches 0 from the left.

in numerical linear power spectra [73, 74, 79]. In addition, a steeper  $k^6$  growth is achievable in models featuring a varying sound speed [80] and for  $\alpha$ -vacuum initial state [81]. Furthermore, it has been demonstrated that scenarios involving multiple transitions during inflation can lead to significantly stronger enhancements [76], a  $k^8$  maximum slope can be realized in the presence of two non-slow-roll phases.

Additionally, a characteristic imprint of the SR-USR transition is the dip structure in the linear power spectrum. This non-trivial feature emerges on the large scales, making it a prominent and observationally accessible signature for testing the USR phase or other non-attractor dynamics [81]. At leading order, Ref. [74] argued that the dip of  $\mathcal{P}_R(k)$  is zero, arising from the exact cancellation between the constant mode and a negative growing mode of  $\mathcal{R}_k$ . This explanation, however, contradicts numerical results that show a non-zero dip. Recently, Ref. [82] employed the  $\delta N$  formalism to analyze the dip structure and the non-linearity in presence of non-attractor phase(s), demonstrating that the conjugate field momentum is crucial for the dip structure. Reference [83] developed a transfer-matrix formalism to study the linear curvature power spectrum in the presence of non-attractor phase(s), showing that the amplitude at the dip always scales as the inverse square root of the peak amplitude.

In this paper, we revisit the linear curvature power spectrum within the conventional SR-USR-SR inflationary framework featuring instantaneous transitions. Adopting the junction method and asymptotic expansions of Hankel functions as in Refs [73, 74], we show that by consistently retaining the dominant contributions, the finite dip in  $\mathcal{P}_R(k)$  can be naturally explained within linear perturbation theory without requiring multiple or smooth transitions. Moreover, we demonstrate that this dip arises from the cancellation between two growing terms in the power spectrum. Additionally, for the first time, we derive appropriate asymptotic expressions that capture the time evolution of power spectra across SR-USR-SR transitions over various  $k$  regimes, as illustrated in Fig. 1. These simple analytical results are straightforward to compute theoretically and provide robust experimental tests, helping impose more reliable constraints on USR inflation with future CMB observations.

The key to deriving accurate asymptotic expressions for the linear curvature power spectrum lies in systematically identifying the dominant contributions. To do so, we propose three simple systematic rules to guide the construction of asymptotic expansions across transitions:

- **Rule 1:** Identify the dominant terms at each transition;
- **Rule 2:** Identify the dominant terms at later times;
- **Rule 3:** Rule 1 must be applied prior to Rule 2.

Notice that, failure to follow Rule 3 may result in the incorrect neglect of dominant terms near transitions, leading to an inaccurate description of the mode function's time evolution. As an example, Eq. (32) will demonstrate that in Case 1 of Fig. 1, a higher-order term in the constant mode can dominate over growing modes at the first SR-USR transition, ultimately producing a finite dip in the subsequent evolution, a subtlety that has largely been overlooked in previous studies.

We begin with a general scenario described by the following EoM for the mode function  $\chi_k$ ,

$$\ddot{\chi}_k + 3\tilde{H}(t)\dot{\chi}_k + \frac{k^2}{a^2}\chi_k = 0, \quad (2)$$

where the Hubble friction coefficient  $\tilde{H}(t)$  has definite asymptotic behaviors:  $\tilde{H}(t) \rightarrow$  positive constants

in both the early-time limit  $t \rightarrow 0$  and the late-time limit  $t \rightarrow \infty$ . The mode  $\chi_k$  may represent the linear comoving curvature perturbation (c.f., Eq. (1)) or the spectator field perturbation during inflation [84–86]. The key challenge is to provide a clear analytical understanding of the resulting power spectrum  $\mathcal{P}_\chi(\tau_{\text{end}}, k) = \frac{k^3}{2\pi^2} |\chi_k(\tau_{\text{end}})|^2$  at the end of inflation. Addressing this challenge hinges on obtaining accurate approximations for the full time evolution of the mode function  $\chi_k(\tau)$ .

This paper is organized as follows. In Sec. 2, we review the Hankel function solutions to the EoM (2) under the quasi-de Sitter approximation. We then introduce the junction method for treating instantaneous transitions and examine the superhorizon and subhorizon asymptotics of Hankel functions, which enable a simple yet precise approximation for the power spectrum  $\mathcal{P}_\chi(\tau, k)$  across different  $k$  regimes. Subsequently, Sec. 3 provides a detailed analysis of the time evolution of  $\mathcal{P}_\chi(\tau, k)$  for the three representative cases of  $k$  regimes illustrated in Fig. 1. Based on the results, we derive analytical expressions for the final power spectrum at the end of inflation. These expressions allow us to explain the characteristic features observed in the spectrum, including the dip,  $k^4$ -growth and wiggles. In Appendix A, we perform a consistent verification of the asymptotic expansions for the power spectra during both the SR and USR phases, utilizing the explicit analytical form of the Hankel functions.

## 2 Analytic Solutions from the Junction Method

### 2.1 General solutions

Applying the quasi-de Sitter approximation  $aH = -\frac{1}{\tau(1-\epsilon)}$  (i.e.,  $\epsilon$  a constant) to Eq. (2), we obtain

$$\chi_k'' + \frac{1-2d}{\tau} \chi_k' + k^2 \chi_k = 0, \quad (3)$$

where the prime refers to the derivatives with respect to the conformal time  $d\tau = dt/a(t)$ . Its solution for a constant  $d \equiv \frac{3h-\epsilon}{2(1-\epsilon)}$ , with  $h \equiv \tilde{H}/H$ , is given by

$$\chi_k(\tau) = A(-\tau)^d H_d^{(1)}(-k\tau) + B(-\tau)^d H_d^{(2)}(-k\tau), \quad (4)$$

where the two unknown coefficients  $A$  and  $B$  can be determined by the initial conditions of  $\chi_k(\tau)$ , or the junction method as we will discuss later.

The main task of this paper is to analyze the asymptotic behaviors of the general solution (4) across SR-USR-SR transitions, as illustrated in the left panel of Fig. 1. The thick gray backslash denotes the comoving Hubble horizon during inflation, while the solid horizontal lines in blue, red and black represent three distinct  $k$  regimes of the mode function  $\chi_k(\tau)$ , corresponding to the classification in the right panel of Fig. 1. The blue dashed line can be interpreted as the boundary of Case 1, corresponding to the  $k$  mode that exits the horizon at the SR-USR transition  $\tau_1$ . Similarly, the black dashed line is regarded as the limit of Case 3, such that the  $k$  mode exits the horizon at the USR-SR transition  $\tau_2$ .

### 2.2 Junction method: SR-USR-SR

One can approximate the non-trivial evolution of the inflationary background as a series of instantaneous transitions with different values of  $d$ , and then match perturbations using smooth

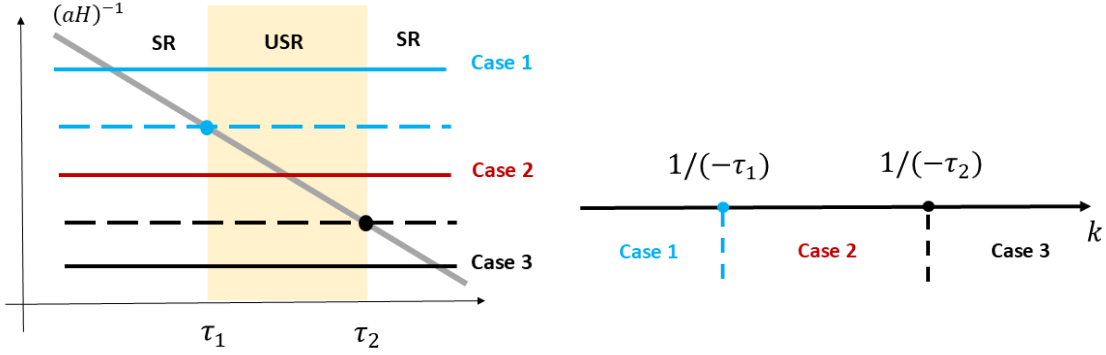


Figure 1: A sketch illustrating three representative  $k$  regimes of the mode function  $\chi_k(\tau)$ , in relation to SR-USR-SR instantaneous transitions denoted by  $\tau_1$  and  $\tau_2$ .

junction conditions. This approach, known as the junction method, has been widely applied to the approximation of linear perturbations, in particular the enhancement of linear perturbations [73, 74, 76, 82, 87–90].

First, we consider a general transition between two phases (also see appendixes in Refs. [73, 87]), i.e.,  $d_1 \rightarrow d_2$ , which have the following two solutions according to Eq. (4),

$$\chi_{1,k}(\tau) = A_1(-\tau)^{d_1} H_{d_1}^{(1)}(-k\tau) + B_1(-\tau)^{d_1} H_{d_1}^{(2)}(-k\tau) , \quad (5a)$$

$$\chi_{2,k}(\tau) = A_2(-\tau)^{d_2} H_{d_2}^{(1)}(-k\tau) + B_2(-\tau)^{d_2} H_{d_2}^{(2)}(-k\tau) , \quad (5b)$$

respectively. Using the junction conditions [73, 74, 91],

$$\chi_{1,k}(\tau_1) = \chi_{2,k}(\tau_1) , \quad \chi'_{1,k}(\tau_1) = \chi'_{2,k}(\tau_1) , \quad (6)$$

with  $\tau_1$  the transition moment, we can solve the coefficients  $\{A_2, B_2\}$  in terms of  $\{A_1, B_1\}$  as

$$\begin{aligned} A_2 &= \frac{1}{4} i\pi A_1 k(-\tau_1)^{d_1-d_2+1} \left[ H_{d_1}^{(1)}(-k\tau_1) H_{d_2-1}^{(2)}(-k\tau_1) - H_{d_1-1}^{(1)}(-k\tau_1) H_{d_2}^{(2)}(-k\tau_1) \right] \\ &\quad + \frac{1}{4} i\pi B_1 k(-\tau_1)^{d_1-d_2+1} \left[ H_{d_1}^{(2)}(-k\tau_1) H_{d_2-1}^{(2)}(-k\tau_1) - H_{d_1-1}^{(2)}(-k\tau_1) H_{d_2}^{(2)}(-k\tau_1) \right] , \end{aligned} \quad (7a)$$

$$\begin{aligned} B_2 &= \frac{1}{4} i\pi A_1 k(-\tau_1)^{d_1-d_2+1} \left[ H_{d_1-1}^{(1)}(-k\tau_1) H_{d_2}^{(1)}(-k\tau_1) - H_{d_1}^{(1)}(-k\tau_1) H_{d_2-1}^{(1)}(-k\tau_1) \right] \\ &\quad + \frac{1}{4} i\pi B_1 k(-\tau_1)^{d_1-d_2+1} \left[ H_{d_1-1}^{(2)}(-k\tau_1) H_{d_2}^{(1)}(-k\tau_1) - H_{d_1}^{(2)}(-k\tau_1) H_{d_2-1}^{(1)}(-k\tau_1) \right] . \end{aligned} \quad (7b)$$

It is clearly that  $A_2, B_2$  are functions of  $k$ . One can iteratively apply the same process and get the solutions for each successive phases, maintaining the same structure of expressions in Eq. (7).

In this paper, we assume the inflation to start from a SR phase and Bunch-Davies vacuum initial state. Applying the de Sitter approximation  $\epsilon = 0$ , we derive the SR solution based on the general solution (4) as  $\chi_k^{\text{SR1}}(\tau) = \frac{H}{\sqrt{2k}} e^{-ik\tau} \left( \frac{i}{k} - \tau \right)$ , i.e.,  $h = 1$ ,  $A = -H\sqrt{\pi}/2$  and  $B = 0$ . Its power spectrum is thus given as

$$\mathcal{P}_\chi^{\text{SR1}}(\tau, k) = \frac{k^3}{2\pi^2} |\chi_k^{\text{SR1}}(\tau)|^2 = \mathcal{P}_{\chi, \text{CMB}} [1 + (-k\tau)^2] , \quad (8)$$

where

$$\mathcal{P}_{\chi, \text{CMB}} \equiv \frac{H^2}{4\pi^2}. \quad (9)$$

Inside the horizon ( $-k\tau \gg 1$ ), the second term dominates, we obtain

$$\mathcal{P}_{\chi}^{\text{SR1}}(\tau, k) \simeq \mathcal{P}_{\chi, \text{CMB}}(-k\tau)^2. \quad (10)$$

At some fixed time, e.g., the end of inflation  $\tau_{\text{end}}$ ,  $\mathcal{P}_{\chi}^{\text{SR1}}(\tau_{\text{end}}, k) \propto k^2$  for the subhorizon modes. On superhorizon scales ( $-k\tau \ll 1$ ), we obtain

$$\mathcal{P}_{\chi}^{\text{SR1}}(\tau, k) \simeq \mathcal{P}_{\chi, \text{CMB}}, \quad (11)$$

which is the famous constant mode of the superhorizon linear perturbations.

Based on solutions in Eq. (7), we consider the transition from SR to USR, such that  $d_1 = 3/2$ ,  $d_2 = -3/2$ . Also, it is sufficient to take the de Sitter limit  $\epsilon = 0$  to the SR solution for our purpose. We obtain

$$A_2 = -\frac{3\sqrt{\pi}H}{4k^3} - \frac{3\sqrt{\pi}H(-\tau_1)^2}{4k} - \frac{i}{2}\sqrt{\pi}H(-\tau_1)^3, \quad (12a)$$

$$B_2 = \frac{3\sqrt{\pi}He^{-2ik\tau_1}}{4k^3} - \frac{3i\sqrt{\pi}H(-\tau_1)e^{-2ik\tau_1}}{2k^2} - \frac{3\sqrt{\pi}H(-\tau_1)^2e^{-2ik\tau_1}}{4k}. \quad (12b)$$

Plugging the above coefficients into the full solution (5b), we obtain the evolution of the mode function after the transition  $\tau_1$ . Similarly, we can derive the coefficients  $A_3$  and  $B_3$  for the last SR phase using the junction method,

$$A_3 = -\frac{\sqrt{\pi}He^{-2ik\tau_1}}{8k^6\tau_2^6} \left[ e^{2ik\tau_1} \left( 2k^3\tau_1^3 + 3ik^2\tau_1^2 + 3i \right) \left( 2k^3\tau_2^3 - 3ik^2\tau_2^2 - 3i \right) - 9e^{2ik\tau_2} (k\tau_1 - i)^2 (k\tau_2 + i)^2 \right], \quad (13a)$$

$$B_3 = \frac{3\sqrt{\pi}He^{-2ik(\tau_1+\tau_2)}}{8k^6\tau_2^6} \left[ e^{2ik\tau_1} \left( -2ik^3\tau_1^3 + 3k^2\tau_1^2 + 3 \right) (k\tau_2 - i)^2 + ie^{2ik\tau_2} (k\tau_1 - i)^2 \left( 2k^3\tau_2^3 + 3ik^2\tau_2^2 + 3i \right) \right]. \quad (13b)$$

In the following discussion, we aim to derive the appropriate asymptotic expressions of the power spectrum  $\mathcal{P}_{\chi}(\tau, k)$  in three distinct  $k$  regimes illustrated in Fig. 1. The asymptotic expressions of  $\mathcal{P}_{\chi}(\tau, k)$  can be derived by expanding the Hankel functions  $H_d^{(1,2)}(-k\tau)$  on either subhorizon ( $-k\tau \gg 1$ ) or superhorizon ( $-k\tau \ll 1$ ) scales. In particular, we first establish that a universal conclusion holds for the superhorizon case, applicable for general  $d$ .

## 2.3 Asymptotics on superhorizon scales: finite growing modes

For a non-integer  $d$ , the power series of Hankel functions are given by [92],

$$H_d^{(1)}(z) = \frac{i\Gamma(d)}{\pi} \sum_{m=0}^{\infty} \frac{(-1)^{m+1} 2^{d-2m}}{m!(1-d)_m} z^{2m-d} + [1 + i \cot(d\pi)] \sum_{m=0}^{\infty} \frac{(-1)^m 2^{-d-2m}}{m!\Gamma(m+d+1)} z^{2m+d}, \quad (14a)$$

$$H_d^{(2)}(z) = -\frac{i\Gamma(d)}{\pi} \sum_{m=0}^{\infty} \frac{(-1)^{m+1} 2^{d-2m}}{m!(1-d)_m} z^{2m-d} + [1 - i \cot(d\pi)] \sum_{m=0}^{\infty} \frac{(-1)^m 2^{-d-2m}}{m!\Gamma(m+d+1)} z^{2m+d}, \quad (14b)$$

which converge rapidly when  $z \ll 1$ , making them well-suited for the asymptotic analysis of mode functions that follows. Here,  $(a)_m \equiv a(a+1)\cdots(a+m-1)$  is the Pochhammer symbol. Plugging Eq. (14) into Eq. (4), we derive

$$\begin{aligned}\chi_k(\tau) &= \frac{i(A-B)\Gamma(d)}{\pi} \sum_{m=0}^{\infty} \frac{(-1)^{m+1} 2^{d-2m}}{m!(1-d)_m} k^{2m-d} (-\tau)^{2m} \\ &\quad + [A+B+i\cot(d\pi)(A-B)] \sum_{m=0}^{\infty} \frac{(-1)^m 2^{-d-2m}}{m!\Gamma(m+d+1)} k^{2m+d} (-\tau)^{2m+2d}.\end{aligned}\quad (15)$$

Examining Eq. (14), the asymptotics of Hankel functions on superhorizon scales (i.e.,  $z \rightarrow 0$ ) can be written concisely as  $H_d^{(1,2)}(z) \rightarrow (z^d, z^{-d}) \times (z^0, z^2, z^4, z^6, \dots)$ , where dots denote higher-order terms in  $z$ , all of which are even powers. Consequently,

$$z^d H_d^{(1,2)}(z) \rightarrow (z^{2d}, z^{2d+2}, z^{2d+4}, z^{2d+6}, \dots) + (z^0, z^2, z^4, z^6, \dots), \quad (16)$$

which demonstrates that only the first branch, the sequence  $(z^{2d}, z^{2d+2}, z^{2d+4}, z^{2d+6}, \dots)$ , can exhibit growth when  $d$  is negative. *Hence, for each such  $d$ , the set of growing modes is necessarily finite.* Because the necessary truncation order depends on the specific problem, no universal prescription can be offered. Each case must be evaluated individually.

In the SR phase with  $d = 3/2$ , Eq. (16) yields  $z^{3/2} H_{3/2}^{(1,2)}(z) \rightarrow (z^3, z^5, z^7, z^9, \dots) + (z^0, z^2, z^4, z^6, \dots)$ , and its squared norm is expressed as

$$\begin{aligned}|z^{3/2} H_{3/2}^{(1,2)}(z)|^2 &\rightarrow z^0 \{z^0 z^0\} + z^2 \{z^0 z^2\} + z^3 \{z^0 z^3\} + z^4 \{z^0 z^4, z^2 z^2\} \\ &\quad + z^5 \{z^0 z^5, z^2 z^3\} + z^6 \{z^0 z^6, z^2 z^4, z^3 z^3\},\end{aligned}\quad (17)$$

where we have dropped irrelevant higher-order terms. Each pair of curly brackets indicates how the corresponding power in the expansion is formed from products of terms in  $|z^{3/2} H_{3/2}^{(1,2)}(z)|^2$ . For instance, the product of terms  $z^0$  and  $z^2$  in  $|z^{3/2} H_{3/2}^{(1,2)}(z)|^2$  gives the mode  $z^2$ . As expected, no growing mode is present in the SR phase. Similarly, in the USR phase with  $d = -3/2$ , Eq. (16) yields

$$\begin{aligned}|z^{-3/2} H_{-3/2}^{(1,2)}(z)|^2 &\rightarrow z^{-6} \{z^{-3} z^{-3}\} + z^{-4} \{z^{-3} z^{-1}\} + z^{-3} \{z^{-3} z^0\} + z^{-2} \{z^{-3} z^1, z^{-1} z^{-1}\} \\ &\quad + z^{-1} \{z^{-3} z^2, z^{-1} z^0\} + z^0 \{z^{-3} z^3, z^{-1} z^1, z^0 z^0\}.\end{aligned}\quad (18)$$

*Hence, retaining terms up to  $z^{2d+6} = z^3$  in  $\chi_k$  suffices to capture all growing modes of the USR solution, as well as the complete constant mode.* Compared with the SR case, the constant mode now receives two additional contributions, i.e.,  $z^{-3} z^3$  and  $z^{-1} z^1$ . The above facts also highlight the importance of mixing terms when considering the asymptotic behaviors of power spectra, which has been missed in previous literature.

Based on the preceding analysis, we calculate the superhorizon asymptotics ( $-k\tau \ll 1$ ) of power spectra in both the SR and USR phases, retaining all relevant terms. Applying the power series (15), in contrast to existing literature, we retain the power spectrum during the SR phase up to the order  $(-\tau)^6$ , and obtain

$$\lim_{-k\tau \ll 1} \mathcal{P}_\chi^{\text{SR}}(\tau, k) \simeq \frac{|A - B|^2}{\pi^3} + \frac{2i(A^*B - AB^*)}{3\pi^3} k^3(-\tau)^3 + \frac{2(A^*B + AB^*)}{9\pi^3} k^6(-\tau)^6. \quad (19)$$

Similarly, in the USR phase with  $d = -3/2$ , the power spectrum is obtained as

$$\begin{aligned} \lim_{-k\tau \ll 1} \mathcal{P}_\chi^{\text{USR}}(\tau, k) &\simeq -\frac{2(AB^* + A^*B)}{9\pi^3} k^6 + \frac{|A|^2 + |B|^2 + 129(A^*B + AB^*)}{2880\pi^3} k^8(-\tau)^2 \\ &\quad + \frac{2i(AB^* - A^*B)}{3\pi^3} k^3(-\tau)^{-3} + \frac{|A + B|^2}{\pi^3} (-\tau)^{-6}, \end{aligned} \quad (20)$$

which includes all growing modes as well as the complete constant mode. And we retain only the leading-order terms that share common coefficients of  $A$  and  $B$ . It should be noted that the limit notation hereafter denotes asymptotic behavior, not a strict mathematical limit.

Additionally, for the SR phase with  $d = 3/2$ , one can show that the power series in Eq. (14) resums to yield,

$$H_{3/2}^{(1)}(z) = e^{iz} z^{-3/2} \sqrt{\frac{2}{\pi}} (-i - z), \quad H_{3/2}^{(2)}(z) = e^{-iz} z^{-3/2} \sqrt{\frac{2}{\pi}} (i - z), \quad (21)$$

and for the USR phase with  $d = -3/2$ , Eq. (14) reduces to

$$H_{-3/2}^{(1)}(z) = ie^{iz} z^{-3/2} \sqrt{\frac{2}{\pi}} (i + z), \quad H_{-3/2}^{(2)}(z) = -ie^{-iz} z^{-3/2} \sqrt{\frac{2}{\pi}} (-i + z). \quad (22)$$

In Appendix A, we demonstrate that all the relevant terms (including the constant mode and growing modes) of power spectra (19) and (20) can be derived consistently from the exact expressions, based on the compact forms in Eqs. (21) and (22).

## 2.4 Asymptotics on subhorizon scales

Beginning with the power series given in Eq. (14), a form suitable for asymptotic analysis on subhorizon scales ( $z \gg 1$ ) can be derived as [92],

$$\begin{aligned} H_d^{(1)}(z) &= \sqrt{\frac{2}{\pi}} e^{i(z - \frac{d\pi}{2} - \frac{\pi}{4})} \left[ z^{-1/2} + \sum_{n=1}^{\infty} \frac{(1/2 - d)_n (1/2 + d)_n}{(2i)^n n!} z^{-n-1/2} \right], \\ H_d^{(2)}(z) &= \sqrt{\frac{2}{\pi}} e^{-i(z - \frac{d\pi}{2} - \frac{\pi}{4})} \left[ z^{-1/2} + \sum_{n=1}^{\infty} \frac{(1/2 - d)_n (1/2 + d)_n}{(-2i)^n n!} z^{-n-1/2} \right]. \end{aligned}$$

Hence, in the subhorizon limit  $-k\tau \gg 1$ , we expand the general solution (4) as

$$\begin{aligned} \lim_{-k\tau \gg 1} \chi_k(\tau) &\simeq \sqrt{\frac{2}{\pi}} \left[ A e^{-ik\tau} e^{-i(\frac{d\pi}{2} + \frac{\pi}{4})} + B e^{ik\tau} e^{i(\frac{d\pi}{2} + \frac{\pi}{4})} \right] k^{-1/2} (-\tau)^{d-1/2} \\ &\quad + \sqrt{\frac{2}{\pi}} \sum_{n=1}^{\infty} \frac{(1/2 - d)_n (1/2 + d)_n}{(2i)^n n!} \left[ A e^{-ik\tau} e^{-i(\frac{d\pi}{2} + \frac{\pi}{4})} + (-1)^n B e^{ik\tau} e^{i(\frac{d\pi}{2} + \frac{\pi}{4})} \right] k^{-n-1/2} (-\tau)^{d-n-1/2}. \end{aligned} \quad (24)$$

Notably, the series expansion in Eq. (24) truncates at  $n = 1$  for both the SR and USR phases, due to the fact that  $(1/2 - d)_2(1/2 + d)_2 = 0$  for  $d = \pm 3/2$ . Hence, we obtain

$$\begin{aligned}\chi_k^{\text{SR}}(\tau) &= \sqrt{\frac{2}{\pi}} \left( -Ae^{-ik\tau} - Be^{ik\tau} \right) k^{-1/2}(-\tau) \\ &\quad + i\sqrt{\frac{2}{\pi}} \left( -Ae^{-ik\tau} + Be^{ik\tau} \right) k^{-3/2},\end{aligned}\tag{25}$$

and

$$\begin{aligned}\chi_k^{\text{USR}}(\tau) &= i\sqrt{\frac{2}{\pi}} \left( Ae^{-ik\tau} - Be^{ik\tau} \right) k^{-1/2}(-\tau)^{-2} \\ &\quad + \sqrt{\frac{2}{\pi}} \left( -Ae^{-ik\tau} - Be^{ik\tau} \right) k^{-3/2}(-\tau)^{-3},\end{aligned}\tag{26}$$

respectively. Importantly, these two expressions already coincide with the exact Hankel functions given in Eqs. (21) and (22). Therefore, we employ the full expressions for the subhorizon asymptotics and omit the limiting notation here.

In the following discussion, we only focus on the expansion at  $n = 1$  in Eq. (24). The power spectrum is thus calculated as

$$\begin{aligned}\mathcal{P}_\chi(\tau, k) &= \frac{1}{\pi^3} k^2 (-\tau)^{2d-1} \left[ X_{\text{non}} + iX_{d,-} \cos(2k\tau) - X_{d,+} \sin(2k\tau) \right] \\ &\quad + \frac{4d^2 - 1}{4\pi^3} k (-\tau)^{2d-2} \left[ X_{d,+} \cos(2k\tau) + iX_{d,-} \sin(2k\tau) \right] \\ &\quad + \frac{1}{\pi^3} \left( \frac{4d^2 - 1}{8} \right)^2 (-\tau)^{2d-3} \left[ X_{\text{non}} - iX_{d,-} \cos(2k\tau) + X_{d,+} \sin(2k\tau) \right],\end{aligned}\tag{27}$$

where  $X_{d,\pm} \equiv A^* B e^{id\pi} \pm AB^* e^{-id\pi}$  represents the amplitudes of oscillations  $\sin(2k\tau)$  and  $\cos(2k\tau)$ , respectively. While  $X_{\text{non}} \equiv |A|^2 + |B|^2$  corresponds to the non-oscillating piece of  $\mathcal{P}_\chi(\tau, k)$ . In the SR phase with  $d = 3/2$ , Eq. (27) gives,

$$\begin{aligned}\mathcal{P}_\chi^{\text{SR}}(\tau, k) &= \frac{1}{\pi^3} k^2 (-\tau)^2 \left[ X_{\text{non}} + iX_{3/2,-} \cos(2k\tau) - X_{3/2,+} \sin(2k\tau) \right] \\ &\quad + \frac{2}{\pi^3} k (-\tau) \left[ iX_{3/2,-} \sin(2k\tau) + X_{3/2,+} \cos(2k\tau) \right] \\ &\quad + \frac{1}{\pi^3} \left[ X_{\text{non}} - iX_{3/2,-} \cos(2k\tau) + X_{3/2,+} \sin(2k\tau) \right],\end{aligned}\tag{28}$$

where  $X_{3/2,\pm} = i(-A^* B \pm AB^*)$ . In the USR phase with  $d = -3/2$ , Eq. (27) gives,

$$\begin{aligned}\mathcal{P}_\chi^{\text{USR}}(\tau, k) &= \frac{1}{\pi^3} k^2 (-\tau)^{-4} \left[ X_{\text{non}} + iX_{-3/2,-} \cos(2k\tau) - X_{-3/2,+} \sin(2k\tau) \right] \\ &\quad + \frac{2}{\pi^3} k (-\tau)^{-5} \left[ X_{-3/2,+} \cos(2k\tau) + iX_{-3/2,-} \sin(2k\tau) \right] \\ &\quad + \frac{1}{\pi^3} (-\tau)^{-6} \left[ X_{\text{non}} - iX_{-3/2,-} \cos(2k\tau) + X_{-3/2,+} \sin(2k\tau) \right],\end{aligned}\tag{29}$$

where  $X_{-3/2,\pm} = -i(-A^* B \pm AB^*)$ .

Based on the superhorizon asymptotics in Eqs. (19) and (20), the subhorizon asymptotics in Eqs. (28) and (29), and the full expressions for coefficients in Eqs. (12) and (13), our next step is to expand the coefficients appearing in these results and retain leading-order contributions. This will allow us to give a clear analytical explanation of the characteristic features of the final power spectrum in distinct  $k$  regimes.

## 3 Time Evolutions of Power Spectra

### 3.1 Case 1

We first examine Case 1 illustrated in Fig. 1, in which the mode exits horizon during the first SR phase, such that  $-k\tau_2 < -k\tau_1 \ll 1$  (or equivalently,  $k \ll 1/(-\tau_1)$ ), where  $\tau_{1,2}$  denote the first and second transition times, respectively. Our goal is to determine appropriate superhorizon asymptotics of the power spectra (19) and (20) during the intermediate USR phase and the last SR phase. In the first SR phase, one can directly apply the results given in Eqs. (8), (10) and (11).

#### 3.1.1 USR

For the USR phase, we evaluate the coefficients in Eq. (20) in the superhorizon limit imposed at the first transition,  $-k\tau_1 \ll 1$ . Following three Rules in Introduction and inserting the exact solutions in Eq. (12) into Eq. (20), we obtain the following leading-order contributions,

$$\lim_{-k\tau_1 \ll 1} (A_2 B_2^* + A_2^* B_2) \simeq -\frac{9\pi H^2}{8} k^{-6} - \frac{9\pi H^2}{4} k^{-4} (-\tau_1)^2, \quad (30a)$$

$$\lim_{-k\tau_1 \ll 1} i (A_2 B_2^* - A_2^* B_2) \simeq -\frac{3\pi H^2}{10} k^{-1} (-\tau_1)^5, \quad (30b)$$

$$\lim_{-k\tau_1 \ll 1} (|A_2|^2 + |B_2|^2 + 129 A_2^* B_2 + 129 A_2 B_2^*) \simeq -144\pi H^2 k^{-6}, \quad (30c)$$

$$\lim_{-k\tau_1 \ll 1} |A_2 + B_2|^2 \simeq \frac{\pi H^2}{25} (-\tau_1)^{10} k^4. \quad (30d)$$

and substituting these expressions into Eq. (20) yields,

$$\begin{aligned} \lim_{-k\tau \ll 1} \mathcal{P}_\chi^{\text{USR}}(\tau, k) \simeq \mathcal{P}_{\chi, \text{CMB}} & \left[ 1 + 2(-\tau_1)^2 k^2 - \frac{1}{5} k^2 (-\tau)^2 \right. \\ & \left. - \frac{4(-\tau_1)^5}{5} k^2 (-\tau)^{-3} + \frac{4(-\tau_1)^{10}}{25} k^4 (-\tau)^{-6} \right]. \end{aligned} \quad (31)$$

Figure 2 shows the comparison between this asymptotic solution (the red dashed curve) and the exact solution (4) with the coefficients (12) (the blue solid curve). We normalize the numerical results by setting  $\tau_1 = -1$  throughout the paper, while the symbolic analyses retain the parameter  $\tau_1$  to ensure generality. Also, we normalize the value  $\mathcal{P}_\chi^{\text{USR}}(\tau, k)$  by the exact value of  $\mathcal{P}_\chi^{\text{USR}}(\tau_1, k)$  in Fig. 2.

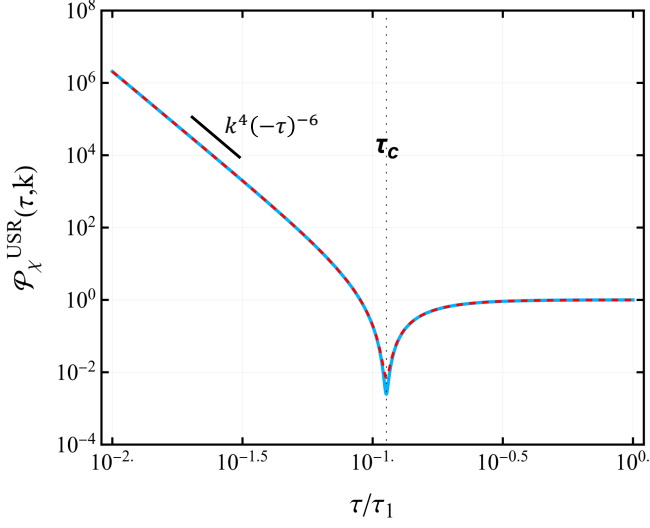


Figure 2: The comparison between the exact solution (4) (the blue solid curve) with coefficients (12), and the asymptotic solution (31) (the red dashed curve), under the parameter choices:  $k = 0.06$ ,  $\tau_1 = -1$ . The value of  $\mathcal{P}_\chi^{\text{USR}}(\tau, k)$  is normalized by the exact value of  $\mathcal{P}_\chi^{\text{USR}}(\tau_1, k)$  based on Eq. (4). The black dotted vertical line refers to the dip time  $\tau_c$  given by Eq. (34). The observed dip structure around  $\tau_c$  emerges from the interplay between the positive  $(-\tau)^{-6}$  term and negative  $(-\tau)^{-3}$  term in Eq. (31).

Following Rule 1&3 in Introduction, one can straightforwardly identify the dominant terms in Eq. (31) at the transition time  $\tau_1$ :

$$\frac{H^2}{4\pi^2} > \frac{H^2}{2\pi^2}(-\tau_1)^2k^2 > \frac{H^2(-\tau_1)^5}{5\pi^2}k^2(-\tau)^{-3} > \frac{H^2}{20\pi^2}k^2(-\tau)^2 > \frac{H^2(-\tau_1)^{10}}{25\pi^2}k^4(-\tau)^{-6}. \quad (32)$$

In contrast to the usual expansion in literature [74], we need to retain the next-to-leading-order  $k$ -dependent term,  $\frac{H^2}{2\pi^2}(-\tau_1)^2k^2$ , in the constant mode of Eq. (31), as well as the decaying  $(-\tau)^2$  mode. At the transition time  $\tau_1$ , the term  $\frac{H^2}{2\pi^2}(-\tau_1)^2k^2$  dominates all other growing modes in Eq. (31), and later produces a finite dip in the time evolution of  $\mathcal{P}_\chi^{\text{USR}}(\tau, k)$ ,<sup>3</sup> see Eq. (35) and Fig. 2. Moreover, Eq. (31) at  $\tau_1$  gives

$$\mathcal{P}_\chi^{\text{USR}}(\tau_1, k) \simeq \mathcal{P}_{\chi, \text{CMB}} [1 + (-k\tau_1)^2], \quad (33)$$

which agrees with the exact SR solution (8), as required by the junction condition (6). This consistency would be lost were the decaying  $(-\tau)^2$  term in Eq. (31) omitted, because this term also dominates the growing  $(-\tau)^{-6}$  mode at the transition, refer to Eq. (32).

The asymptotic power spectrum (31) shows that the dominant late-time growth is carried by the growing  $(-\tau)^{-6}$  mode with a  $k^4$ -dependence, see Fig. 2. Crucially, the negative  $(-\tau)^{-3}$  term dominates over the  $(-\tau)^{-6}$  term initially, refer to Eq. (32). Then after the transition, the  $(-\tau)^{-3}$  term first cancels the constant mode  $\mathcal{P}_{\chi, \text{CMB}} [1 + 2(-\tau_1)^2k^2]$ , until the difference between the  $(-\tau)^{-6}$  and  $(-\tau)^{-3}$  terms attains its extremum, leading to the dip structure as shown in Fig. 2. Then, we can calculate the corresponding dip time as

<sup>3</sup>The decaying  $(-\tau)^2$  term is negligible at the dip time  $\tau_c$  defined by Eq. (34).

$$\tau_c = -\left(\frac{2}{5}\right)^{1/3} k^{2/3} (-\tau_1)^{5/3}, \quad (34)$$

indicated by the black dotted vertical lines in Fig. 2, and in excellent agreement with the exact result (the blue solid curve). Then, we calculate the dip value as

$$\mathcal{P}_\chi^{\text{USR}}(\tau_c, k) \simeq 2\mathcal{P}_{\chi, \text{CMB}}(-k\tau_1)^2, \quad (35)$$

which is finite. Note that  $-\tau_c < -\tau_1$  holds for  $-k\tau_1 < 1$ , meaning the dip of the time evolution of USR mode always exists after the transition time  $\tau_1$  (as far as the USR phase lasts sufficiently long duration, refer to Fig. 4) in Case 1.

### 3.1.2 SR2

At the second transition time  $\tau_2$ , we require the superhorizon asymptotics of the coefficients in Eq. (13) under  $-k\tau_2 < -k\tau_1 \ll 1$ . Treating it as a two-parameter expansion, we introduce two small bookkeeping parameters,  $x \equiv -k\tau_1$  and  $y \equiv -k\tau_2$ , where  $y < x \ll 1$ . Then, we rewrite  $A_3$  and  $B_3$  in Eq. (13) as

$$A_3 = -\frac{\sqrt{\pi}He^{2ix}}{8y^6} \left[ e^{-2ix} \left( -2x^3 + 3ix^2 + 3i \right) \left( -2y^3 - 3iy^2 - 3i \right) - 9e^{-2iy}(-x-i)^2(-y+i)^2 \right], \quad (36a)$$

$$B_3 = \frac{3\sqrt{\pi}He^{2i(x+y)}}{8y^6} \left[ e^{-2ix} \left( 2ix^3 + 3x^2 + 3 \right) (-y-i)^2 + ie^{-2iy}(-x-i)^2 \left( -2y^3 + 3iy^2 + 3i \right) \right]. \quad (36b)$$

Expanding to the leading order in  $y < x \ll 1$  gives

$$\lim_{-k\tau_2 < -k\tau_1 \ll 1} |A_3 - B_3|^2 \simeq \pi H^2 \left[ \frac{1}{4} + \frac{1}{2}k^2(-\tau_1)^2 - \frac{2}{5}\frac{(-\tau_1)^5}{(-\tau_2)^3}k^2 + \frac{4}{25}\frac{(-\tau_1)^{10}}{(-\tau_2)^6}k^4 \right], \quad (37a)$$

$$\lim_{-k\tau_2 < -k\tau_1 < 1} i(A_3^*B_3 - A_3B_3^*) \simeq \pi H^2 \left[ -\frac{6}{25}\frac{(-\tau_1)^{10}}{(-\tau_2)^9}k + \frac{3}{10}\frac{(-\tau_1)^5}{(-\tau_2)^6}k^{-1} \right], \quad (37b)$$

$$\lim_{-k\tau_2 < -k\tau_1 < 1} (A_3^*B_3 + A_3B_3^*) \simeq \frac{9\pi H^2}{50}\frac{(-\tau_1)^{10}}{(-\tau_2)^{12}}k^{-2}. \quad (37c)$$

Inserting these expressions into Eq. (19) yields

$$\begin{aligned} \lim_{-k\tau \ll 1} \mathcal{P}_\chi^{\text{SR2}}(\tau, k) &\simeq \mathcal{P}_{\chi, \text{CMB}} \left\{ \left[ 1 + 2k^2(-\tau_1)^2 - \frac{8}{5}\frac{(-\tau_1)^5}{(-\tau_2)^3}k^2 + \frac{16}{25}\frac{(-\tau_1)^{10}}{(-\tau_2)^6}k^4 \right] \right. \\ &\quad \left. + \left[ -\frac{16}{25}\frac{(-\tau_1)^{10}}{(-\tau_2)^9}k^4 + \frac{4}{5}\frac{(-\tau_1)^5}{(-\tau_2)^6}k^2 \right] (-\tau)^3 + \frac{4(-\tau_1)^{10}}{25(-\tau_2)^{12}}k^4(-\tau)^6 \right\}. \end{aligned} \quad (38)$$

In contrast to the USR asymptotic solution (31), we keep more terms in Eq. (38), because the unconstrained ratio  $\tau_2/\tau_1$  makes it impossible to identify dominant terms at the second transition

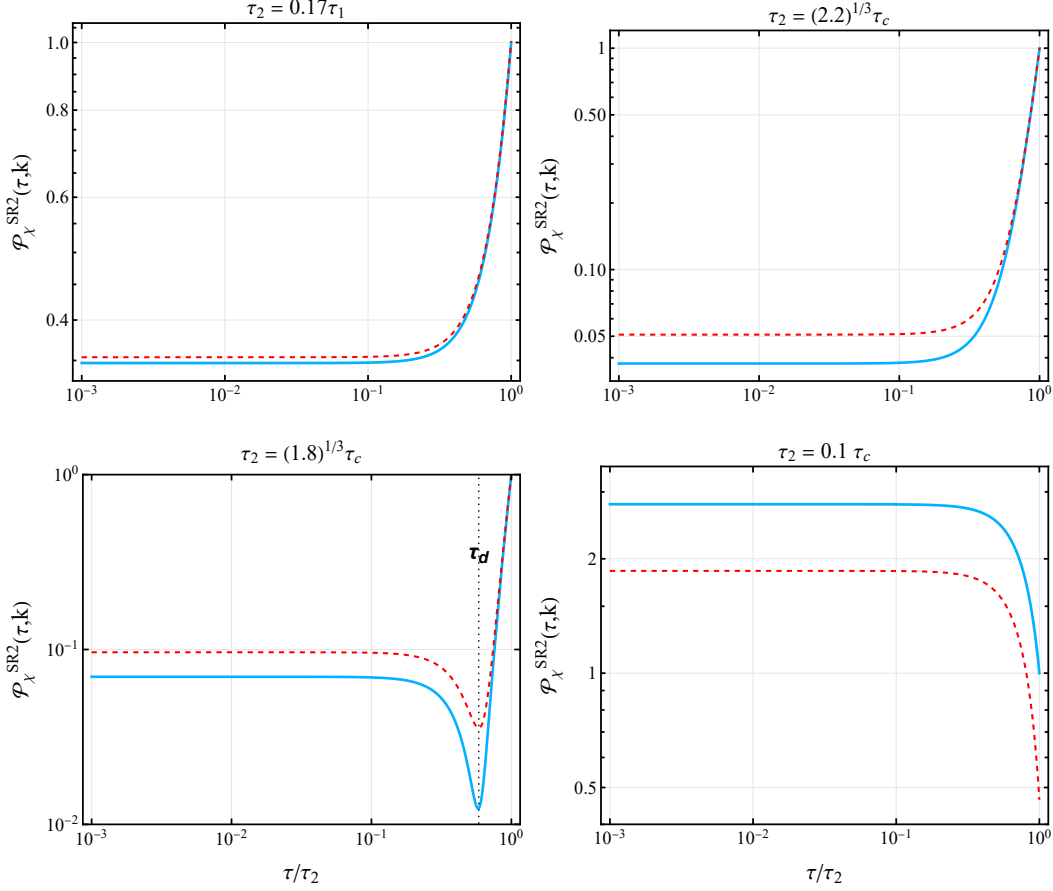


Figure 3: The comparisons between the exact solution (4) (the blue solid curves) with the coefficients (13), and the asymptotic power spectrum (38) (the red dashed curves), for  $k = 0.06$  and  $\tau_1 = -1$  with  $\tau_2$  scaled as  $0.17\tau_1$ ,  $(2.2)^{1/3}\tau_1$ ,  $(1.8)^{1/3}\tau_1$ ,  $0.1\tau_1$ . All the results are normalized by the exact value of  $\mathcal{P}_\chi^{\text{SR2}}(\tau_2, k)$  based on Eq. (4). The dip time  $\tau_d$  is given by Eq. (40), which only exists when  $-\tau_2 < -2^{1/3}\tau_c$ .

time  $\tau_2$ . Crucially, the sign of  $(-\tau)^3$  term in Eq. (38) is determined by the expressions inside the square bracket: it is negative for  $-\tau_c \lesssim -\tau_2 < -2^{1/3}\tau_c$  and positive for  $-2^{1/3}\tau_c \lesssim -\tau_2 < -\tau_1$ . It is this sign flip that governs the qualitative shape of  $\mathcal{P}_\chi^{\text{SR2}}(\tau, k)$ , refer to Fig. 3.

Before examining the ratio  $\tau_2/\tau_1$ , we first calculate the power spectrum at the transition time  $\tau_2$  based on Eq. (38), and obtain

$$\mathcal{P}_\chi^{\text{SR2}}(\tau_2, k) \simeq \mathcal{P}_{\chi, \text{CMB}} \left[ 1 + 2k^2(-\tau_1)^2 - \frac{4}{5} \frac{(-\tau_1)^5}{(-\tau_2)^3} k^2 + \frac{4}{25} \frac{(-\tau_1)^{10}}{(-\tau_2)^6} k^4 \right], \quad (39)$$

which is approximated to the calculation from Eq. (31) at  $\tau_2$  by discarding the negligible term  $H^2 k^2 (-\tau_2)^2 / (20\pi^2)$  arising from the  $(-\tau)^2$  term in Eq. (31).

Now, we examine the the asymptotic evolution of  $\mathcal{P}_\chi^{\text{SR2}}(\tau, k)$  given by Eq. (38) in terms of the varied ratio  $\tau_2/\tau_1$  for given  $\tau_1$  and  $k$ .

1.  $-2^{2/3}\tau_c < -\tau_2 < -\tau_1$ ,<sup>4</sup> the constant mode dominates the asymptotic behavior of Eq. (38)

<sup>4</sup>According to Eq. (34), it is easy to check that  $-2^{2/3}\tau_c < -\tau_1$  for  $-k\tau_1 \ll 1$ .

(expressed for simplicity as  $(-\tau)^0 > (-\tau)^3 > (-\tau)^6$ ), which corresponds to a quite short USR phase (see the top-left panel of Fig. 4), which leaves the mode function almost unchanged. The power spectrum at the end of inflation can be calculated either by utilizing the constant mode from Eq. (31), or by evaluating the USR solution at  $\tau_2$  under the approximation  $\tau_2 \simeq \tau_1$ , both approaches yield identical results. We obtain  $\mathcal{P}_\chi^{\text{SR2}}(\tau_{\text{end}}, k) \simeq H^2/(4\pi^2) = \mathcal{P}_{\chi, \text{CMB}}$  as expected.

2.  $-3^{1/3}\tau_c < -\tau_2 < -2^{2/3}\tau_c$ , we have  $(-\tau)^3 > (-\tau)^0 > (-\tau)^6$  at  $\tau_2$ , and the  $(-\tau)^3$  term is positive. Hence, the power spectrum  $\mathcal{P}_\chi^{\text{SR2}}(\tau, k)$  first falls off as  $(-\tau)^3$  and then settles onto the constant plateau given by Eq. (44). The power spectrum (38) is shown by the red dashed curve in the top-left panel of Fig. 3, along with the exact solution (4) with the coefficients (13) represented by the blue solid curve. All results in Fig. 3 are normalized by the exact value of  $\mathcal{P}_\chi^{\text{SR2}}(\tau_2, k)$  based on Eq. (4).

3.  $-\left(\frac{5}{2}\right)^{1/3}\tau_c < -\tau_2 < -3^{1/3}\tau_c$ , we have  $(-\tau)^3 > (-\tau)^6 > (-\tau)^0$  at  $\tau_2$ , and the  $(-\tau)^3$  term is positive. The overall evolution is similar to the previous case.

4.  $-2^{1/3}\tau_c < -\tau_2 < -\left(\frac{5}{2}\right)^{1/3}\tau_c$ , we have  $(-\tau)^6 > (-\tau)^3 > (-\tau)^0$  at  $\tau_2$ , and the  $(-\tau)^3$  term remains positive. The power spectrum  $\mathcal{P}_\chi^{\text{SR2}}(\tau, k)$  first decays as  $(-\tau)^6$ , then switches to a  $(-\tau)^3$  fall-off before finally settling at the constant plateau given by Eq. (44). This evolution is illustrated in the top-right panel of Fig. 3.

5.  $-\tau_c < -\tau_2 < -2^{1/3}\tau_c$ , we have  $(-\tau)^6 > (-\tau)^0 > (-\tau)^3$  at  $\tau_2$ , and the  $(-\tau)^3$  term turns negative. This case is similar to that is shown in Fig. 2. The power spectrum  $\mathcal{P}_\chi^{\text{SR2}}(\tau, k)$  first falls as  $(-\tau)^6$ , and is simultaneously driven lower by the negative  $(-\tau)^3$  term. The dip appears when the sum of the  $(-\tau)^6$  and  $(-\tau)^3$  terms in Eq. (38) reaches its minimum (as shown by the black dotted line in the bottom-left panel of Fig. 3), and we thus calculate the dip time as

$$\tau_d = 2^{-1/3}\tau_2 \left[ 4 - 5k^{-2} \frac{(-\tau_2)^3}{(-\tau_1)^5} \right]^{1/3}. \quad (40)$$

The corresponding dip value is calculated as

$$\mathcal{P}_\chi^{\text{SR2}}(\tau_d, k) \simeq 2\mathcal{P}_{\chi, \text{CMB}}(-k\tau_1)^2, \quad (41)$$

which is the same with Eq. (35) by accident. Note that  $\tau_d$  only exists when  $-\tau_2 < -2^{1/3}\tau_c$ , and  $-\tau_d < -\tau_c < -\tau_2$  always holds for  $-\tau_c < -\tau_2 < -2^{1/3}\tau_c$  based on the expression (40), which is clearly shown in the middle-left panel of Fig. 4. Ultimately,  $\mathcal{P}_\chi^{\text{SR2}}(\tau, k)$  settles to the constant plateau given by Eq. (44). This evolution is shown in the bottom-left panel of Fig. 3. Moreover, we find

$$\tau_d = \tau_c \text{ when } \tau_2 = \tau_c, \quad (42)$$

which means that if the second transition is chosen as  $\tau_2 = \tau_c$ , we obtain

$$\tau_2 = \tau_c = \tau_d \quad \text{and} \quad \mathcal{P}_\chi^{\text{SR2}}(\tau_{\text{end}}, k) = \mathcal{P}_\chi^{\text{USR}}(\tau_1, k), \quad (43)$$

as shown in the middle-right panel of Fig. 4. The presence of such a USR phase does not lead to any change of the power spectrum at the end of inflation, corresponding to a typical scale  $\sqrt{2}k_{\text{dip}}$ , as we will discuss in Eq. (47) and Fig. 5.

6.  $0 < -\tau_2 < -\tau_c$ , we have  $(-\tau)^0 > (-\tau)^6 > (-\tau)^3$  at  $\tau_2$ , and  $\tau_d$  does not exist anymore, which means the damping effects arising from the negative  $(-\tau)^3$  term becomes weaker, the power spectrum

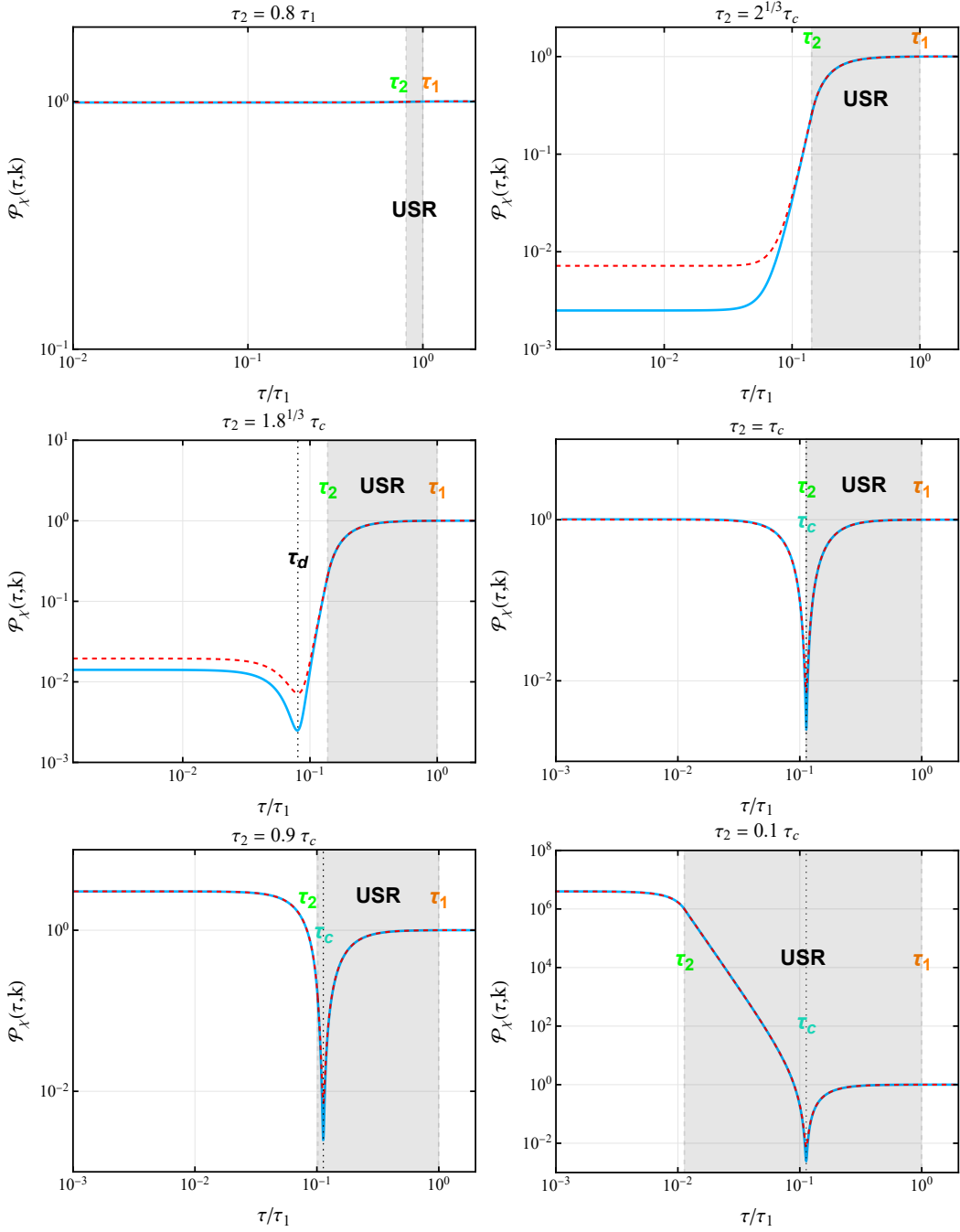


Figure 4: Time evolutions of the power spectrum  $\mathcal{P}_\chi(\tau, k)$  across SR-USR-SR transitions, corresponding to Case 1 of Fig. 1 for  $\tau_2 = 0.8\tau_1, 2^{1/3}\tau_c, 1.8^{1/3}\tau_c, \tau_c, 0.9\tau_c, 0.1\tau_c$ , respectively. The blue solid curves denote the exact solutions of power spectra based on Eqs. (4), (12) and (13), while the red dashed curves represent the asymptotic solutions given by Eqs. (8), (31) and (38). All results are normalized by the exact value of  $\mathcal{P}_\chi^{\text{USR}}(\tau_1, k)$  based on Eq. (4). The dip times  $\tau_c$  and  $\tau_d$  are defined in Eqs. (34) and (40), respectively.

$\mathcal{P}_\chi^{\text{SR2}}(\tau, k)$  grows slightly after the transition  $\tau_2$ , and quickly settles to the constant value given by Eq. (44), as shown in the bottom-right panel of Fig. 3. Importantly, only this regime displays the enhancement of the power spectrum, refer to the bottom-left and -right panels of Fig. 4.

At the end of inflation  $\tau_{\text{end}}$ , the constant mode must dominate, giving

$$\mathcal{P}_\chi^{\text{SR2}}(\tau_{\text{end}}, k) \simeq \mathcal{P}_{\chi, \text{CMB}} \left[ 1 + 2k^2(-\tau_1)^2 - \frac{8}{5} \frac{(-\tau_1)^5}{(-\tau_2)^3} k^2 + \frac{16}{25} \frac{(-\tau_1)^{10}}{(-\tau_2)^6} k^4 \right], \quad (44)$$

which encodes the duration of the USR phase. Equating Eqs. (33) and (44) yields the necessary condition for the enhancement of the power spectrum with respect to the vanilla SR inflation, we derive the equal time as

$$\tau_2^{\text{eq}} \simeq - \left( \frac{2}{5} \right)^{1/3} k^{2/3} (-\tau_1)^{5/3} = \tau_c. \quad (45)$$

The enhancement of  $\mathcal{P}_\chi^{\text{SR2}}(\tau_{\text{end}}, k)$  therefore requires the second transition to occur after the USR dip, i.e.,  $-\tau_2 < -\tau_c$ . This is natural: because the power spectrum (31) of USR phase begins to grow only after the dip time  $\tau_c$  (c.f., Fig. 2), and no growing mode persists after the USR phase, as shown in Eq. (38).

In summary, the asymptotic solutions of  $\mathcal{P}_\chi(\tau, k)$  for  $k \ll 1/(-\tau_1)$  are provided in Eqs. (8), (31) and (38). These asymptotic results coincide with the exact solutions (given in Eqs. (4), (12) and (13)), as demonstrated in Fig. 4 by the red dashed and blue solid curves, respectively. The critical time  $\tau_c$ , defined in Eq. (34), emerges from the interplay between the positive growing  $(-\tau)^{-6}$  mode and negative growing  $(-\tau)^{-3}$  mode of the USR power spectrum (31). It determines the second transition time  $\tau_2$  that separates parameter regions, in which the final power spectrum  $\mathcal{P}_\chi^{\text{SR2}}(\tau_{\text{end}}, k)$  is enhanced or suppressed relative to the exact value of  $\mathcal{P}_\chi^{\text{SR1}}(\tau_1, k)$  (equivalently  $\mathcal{P}_\chi^{\text{USR}}(\tau_1, k)$ ):

$$\begin{aligned} -\tau_c < -\tau_2 < -2^{2/3}\tau_c, & \quad \text{suppression;} \\ -2^{2/3}\tau_c \ll -\tau_2 \text{ and } -\tau_2 = -\tau_c, & \quad \text{plateau;} \\ 0 < -\tau_2 < -\tau_c, & \quad \text{enhancement.} \end{aligned} \quad (46)$$

In other words, the qualitative behaviors of time evolution of the power spectrum across SR-USR-SR transitions is determined by  $\tau_{1,2}$  and  $k$ .

### 3.1.3 The dip structure of the final power spectrum

Notably, while the preceding analysis is carried out for a fixed  $k$ , the variation of final power spectrum (44) with respect to  $k$  can be inferred directly from the conclusion (46). This is because  $\tau_c$  depends on  $k$  (c.f., Eq. (34)), while  $\tau_{1,2}$  are  $k$ -independent model parameters that accompany with  $k$  in the combination  $-k\tau_{1,2}$ . Consequently, given transition times  $\tau_{1,2}$  map to different dynamical regimes depending on the value of  $k$ . The classification (46) is therefore equivalent to

$$\begin{aligned} \frac{1}{\sqrt{2}}k_{\text{dip}} < k < \sqrt{2}k_{\text{dip}}, & \quad \text{suppression,} \\ k \ll \frac{1}{\sqrt{2}}k_{\text{dip}} \text{ and } k = \sqrt{2}k_{\text{dip}}, & \quad \text{plateau,} \\ \sqrt{2}k_{\text{dip}} < k < 1/(-\tau_1), & \quad \text{enhancement.} \end{aligned} \quad (47)$$

As illustrated in Fig. 5, the final power spectrum  $\mathcal{P}_\chi^{\text{SR2}}(\tau_{\text{end}}, k)$  in Eq. (44) exhibits a nearly scale-invariant in the small  $k$ -regime, and transitions to a  $k^4$ -growth in the relative large  $k$ -regime. That is, the term  $\frac{16}{25} \frac{(-\tau_1)^{10}}{(-\tau_2)^6} k^4$  in Eq. (44) dominates in the large  $k$ -regime.

The dip scale  $k_{\text{dip}}$  in Eq. (47), is obtained from the equation  $\frac{\partial}{\partial k} [\mathcal{P}_\chi^{\text{SR2}}(\tau_{\text{end}}, k)] \Big|_{k=k_{\text{dip}}} = 0$ , such that

$$k_{\text{dip}} \simeq \frac{\sqrt{5}}{2} \frac{(-\tau_2)^{3/2}}{(-\tau_1)^{5/2}}, \quad (48)$$

or equivalently,

$$(-k_{\text{dip}}\tau_1)^2 \simeq \frac{5}{4} e^{-3N_{\text{USR}}}. \quad (49)$$

where  $N_{\text{USR}} \simeq \ln(\tau_1/\tau_2)$  is the e-folding number of the intermediate USR phase. The second derivative at  $k_{\text{dip}}$  is positive, meaning  $k_{\text{dip}}$  refers to a minimum, i.e., the dip position of the final power spectrum  $\mathcal{P}_\chi^{\text{SR2}}(\tau_{\text{end}}, k)$  for fixed  $\tau_{1,2}$ , as shown in Fig. 5. This dip scale  $k_{\text{dip}}$  arises from the cancellation between the terms  $-\frac{8}{5} \frac{(-\tau_1)^5}{(-\tau_2)^3} k^2$  and  $\frac{16}{25} \frac{(-\tau_1)^{10}}{(-\tau_2)^6} k^4$  in Eq. (44). This cancellation, in turn, stems from the interplay between the positive  $(-\tau)^{-6}$  term and negative  $(-\tau)^{-3}$  term of the USR power spectrum (31).

It is straightforward to verify that the analytical expressions for the dip position given above in Eqs. (48) and (49) are consistent with the existing literature. Our advance is to provide the first simple analytical forms for these quantities, offering a novel analytical toolkit for theoretical work. From Eq. (48) and the final power spectrum peak that we will discuss in Eq. (72), we derive the relationship between the dip position and the peak value as,

$$-k_{\text{dip}}\tau_1 \propto (\mathcal{P}_{\chi,\text{pk}})^{-1/4}, \quad (50)$$

which matches with Eq. (3.9) given in Ref. [76]. For an enhancement of the power spectrum peak by approximately  $10^7$  (c.f., Eq. (73) with  $N_{\text{USR}} \simeq 2.36$ ), Eq. (49) yields  $k/k_1 \simeq 0.0324$ , where  $k_1 \equiv 1/(-\tau_1)$ . This is consistent with the result of 0.0367 reported in Ref. [82]. Finally, based on Eq. (44), another relationship is obtained,

$$k_{\text{dip}}^2 \simeq -2 \frac{k_1^2}{A_2}, \quad (51)$$

where  $A_2 = -\frac{8}{5} \frac{(-\tau_1)^3}{(-\tau_2)^3}$  is the coefficient of  $k^2$  term in Eq. (44), as defined in Eq. (5.14) of Ref. [83]. Equation (51) agrees with Eq. (5.16) in Ref. [83], except for a factor of 2. Reference [83] also claimed that Eq. (51) leads to a existence criterion of  $k_{\text{dip}}$ , such that  $A_2 < 0$  corresponding to the inflation velocity does not flip its sign.

The corresponding dip value can be evaluated from Eq. (44) as

$$\mathcal{P}_{\chi,\text{dip}} \equiv \mathcal{P}_\chi^{\text{SR2}}(\tau_{\text{end}}, k_{\text{dip}}) \simeq \frac{5}{2} \mathcal{P}_{\chi,\text{CMB}} e^{-3N_{\text{USR}}}, \quad (52)$$

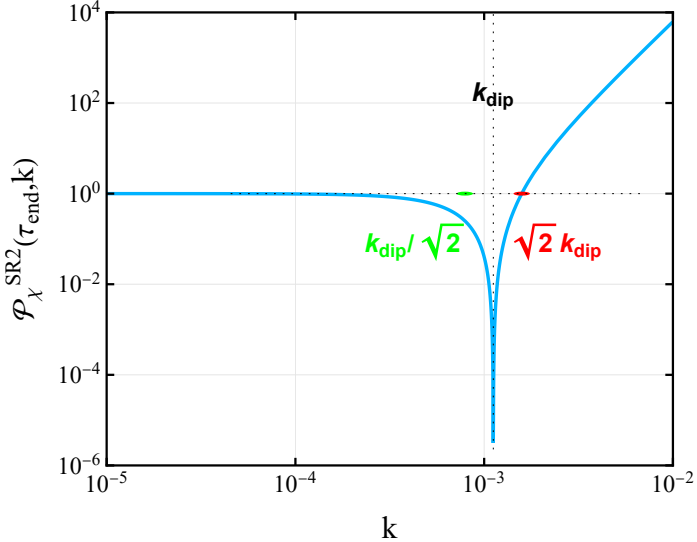


Figure 5: The final power spectrum  $\mathcal{P}_\chi^{\text{SR2}}(\tau_{\text{end}}, k)$  in Eq. (44) with  $\tau_2 = 10^{-2}\tau_1 = -0.01$ , which features a dip at  $k_{\text{dip}}$  expressed in Eq. (48) or equivalently Eq. (49). The spectrum is nearly scale-invariant for  $k \ll k_{\text{dip}}/\sqrt{2}$ , and transitions to a  $k^4$  growth for  $k > \sqrt{2}k_{\text{dip}}$ . The value of  $\mathcal{P}_\chi^{\text{SR2}}(\tau_{\text{end}}, k)$  is normalized by  $\mathcal{P}_\chi^{\text{USR}}(\tau_1, k)$  based on Eq. (4).

which is finite and consistent with the numerical results from the linear perturbation theory [71, 73–77]. This value originates from the sub-leading term  $k^2(-\tau_1)^2$  in Eq. (44), while the remaining terms cancel exactly. Combining the dip value (52) and the peak value (72), we derive the relation,

$$\frac{\mathcal{P}_{\chi, \text{dip}}}{\mathcal{P}_{\chi, \text{CMB}}} \propto \left( \frac{\mathcal{P}_{\chi, \text{pk}}}{\mathcal{P}_{\chi, \text{CMB}}} \right)^{-1/2}, \quad (53)$$

which has been reported in Eq. (3.9) of Ref. [76] as well as Eq. (5.20) of Ref. [83].

What then sets the upper bound on the attainable enhancement? From the expression (44), the enhancement magnitude scales inversely with  $-\tau_2$  for given  $\tau_1$  and  $k$ . That is, a longer USR phase yields stronger amplification. Moreover, Eq. (44) shows that  $\mathcal{P}_\chi^{\text{SR2}}(\tau_{\text{end}}, k)$  is proportional to  $k$ . However, for fixed  $\tau_{1,2}$  in Case 1,  $k$  is bounded by  $-k\tau_2 < -k\tau_1 \ll 1$ . Hence, the peak position  $k_{\text{pk}}$  of the final power spectrum  $\mathcal{P}_\chi^{\text{SR2}}(\tau_{\text{end}}, k)$  must arise in other Cases of Fig. 1.

### 3.2 Case 3

Now, we consider Case 3 of Fig. 1, such that the  $k$  mode exists the horizon during the last SR phase, meaning it remains subhorizon throughout both the first SR phase and the subsequent USR phase. Thus, we have the relationship  $-k\tau_1 > -k\tau_2 \gg 1$  for Case 3.

For the first SR phase,  $d = 3/2$ ,  $A = -H\sqrt{\pi}/2$  and  $B = 0$ , and we have  $X_{3/2,\pm} = 0$ , Eq. (28) therefore gives

$$\lim_{-k\tau \gg 1} \mathcal{P}_\chi^{\text{SR1}}(\tau, k) \simeq \frac{1}{\pi^2} k^2 (-\tau)^2 X_{\text{non}}^{\text{SR1}}(k) \simeq \mathcal{P}_{\chi, \text{CMB}}(-k\tau)^2, \quad (54)$$

which matches with Eq. (10).

In the subsequent USR phase, we derive the following asymptotic expansions according to Eq. (12),

$$\lim_{-k\tau_1 \gg 1} (|A_2|^2 + |B_2|^2) \simeq \frac{H^2 \pi (-\tau_1)^6}{4}, \quad (55a)$$

$$\lim_{-k\tau_1 \gg 1} (A_2^* B_2 + A_2 B_2^*) \simeq \frac{3H^2 \pi (-\tau_1)^5 \sin(-2k\tau_1)}{4k}, \quad (55b)$$

$$\lim_{-k\tau_1 \gg 1} i (A_2^* B_2 - A_2 B_2^*) \simeq \frac{3H^2 \pi (-\tau_1)^5 \cos(2k\tau_1)}{4k}. \quad (55c)$$

These imply that the amplitude  $X_{-3/2,\pm}$  of oscillatory terms in Eq. (28) is negligible relative to the non-oscillating amplitude  $X_{\text{non}}(k)$  for  $-k\tau_1 \gg 1$ . By substituting coefficients in Eq. (55) into the asymptotic expression (29), we derive

$$\lim_{-k\tau \gg 1} \mathcal{P}_\chi^{\text{USR}}(\tau, k) \simeq \mathcal{P}_{\chi, \text{CMB}}(-\tau_1)^6 k^2 (-\tau)^{-4}, \quad (56)$$

which indicates that the USR power spectrum on subhorizon scales exhibits a growing mode  $k^2(-\tau)^{-4}$ . At the transition  $\tau_1$ , Eq. (56) gives

$$\lim_{-k\tau \gg 1} \mathcal{P}_\chi^{\text{USR}}(\tau_1, k) \simeq \mathcal{P}_{\chi, \text{CMB}}(-k\tau_1)^2, \quad (57)$$

which matches the preceding SR result (54), as expected from the junction condition (6).

During the final SR phase, the mode exits the horizon at a later time. Similar to Sec. 3.1.2, treating it as a two-parameter problem, we determine the leading-order terms of the coefficients in Eq. (13) as

$$\lim_{-k\tau_1 > -k\tau_2 \gg 1} (|A_3|^2 + |B_3|^2) \simeq \frac{H^2 \pi}{4} \frac{(-\tau_1)^6}{(-\tau_2)^6}, \quad (58a)$$

$$\lim_{-k\tau_1 > -k\tau_2 \gg 1} (A_3^* B_3 + A_3 B_3^*) \simeq \frac{3H^2 \pi}{4} \frac{(-\tau_1)^6 \sin(-2k\tau_2)}{k(-\tau_2)^7}, \quad (58b)$$

$$\lim_{-k\tau_1 > -k\tau_2 \gg 1} i (A_3^* B_3 - A_3 B_3^*) \simeq \frac{3H^2 \pi}{4} \frac{(-\tau_1)^6 \cos(-2k\tau_2)}{k(-\tau_2)^7}. \quad (58c)$$

If the  $k$  mode remains deep inside the horizon at the second transition  $\tau_2$ , such that  $-k\tau_2 \gg 1$ , the non-oscillating amplitude  $X_{\text{non}}^{\text{SR2}}(k)$  also dominates over the oscillating amplitude  $X_{3/2,\pm}$  (c.f., the left panel of Fig. 6). Conversely, if the mode exits the horizon shortly after  $\tau_2$ ,  $X_{3/2,\pm}$  becomes comparable to  $X_{\text{non}}^{\text{SR2}}(k)$ , as illustrated in the right panel of Fig. 6. Inserting expressions in Eq. (58) into the exact solution (28) gives the leading expression,

$$\begin{aligned} & \mathcal{P}_\chi^{\text{SR2}}(\tau, k) \\ & \simeq \frac{H^2}{4\pi^2} \frac{(-\tau_1)^6}{(-\tau_2)^6} \left\{ 1 + \left[ k^2 + 3 \frac{\sin(-2k\tau_2)}{-\tau_2} k \cos(2k\tau) + 3 \frac{\cos(-2k\tau_2)}{-\tau_2} k \sin(2k\tau) \right] (-\tau)^2 \right\}, \end{aligned} \quad (59)$$

where we have dropped the  $(-\tau)$  term in Eq. (28) as it is subdominant: compared to the  $(-\tau)^2$  term on subhorizon scales, and to the constant mode (i.e., the third line in Eq. (28)) on superhorizon

scales. In addition, the non-oscillatory part  $X_{\text{non}}$  dominates all other oscillating parts in the constant mode on superhorizon scales. The red dashed curves in Fig. 6 denote the asymptotic expressions given in Eqs. (54), (56) and (59), while the blue solid curves represent the exact solutions based on Eq. (4) with the coefficients (13).

To verify consistency, we apply Eq. (59) to derive the initial value at the transition  $\tau_2$ ,

$$\mathcal{P}_\chi^{\text{SR2}}(\tau_2, k) \simeq \mathcal{P}_{\chi, \text{CMB}} \frac{(-\tau_1)^6}{(-\tau_2)^4} k^2, \quad (60)$$

which matches the results derived from Eq. (56).

According to Eq. (59), we calculate the final value as

$$\mathcal{P}_\chi^{\text{SR2}}(\tau_{\text{end}}, k) \simeq \mathcal{P}_{\chi, \text{CMB}} e^{6N_{\text{USR}}}. \quad (61)$$

Alternatively, the same result can be derived from the constant mode in the superhorizon asymptotics (19), i.e.,  $\lim_{k\tau \ll 1} \mathcal{P}_\chi^{\text{SR2}}(\tau, k) \simeq 2|A_3 - B_3|^2/\pi$ , with the leading-order contribution  $|A_3 - B_3|^2 \simeq \frac{H^2\pi}{4} \frac{(-\tau_1)^6}{(-\tau_2)^6}$ .

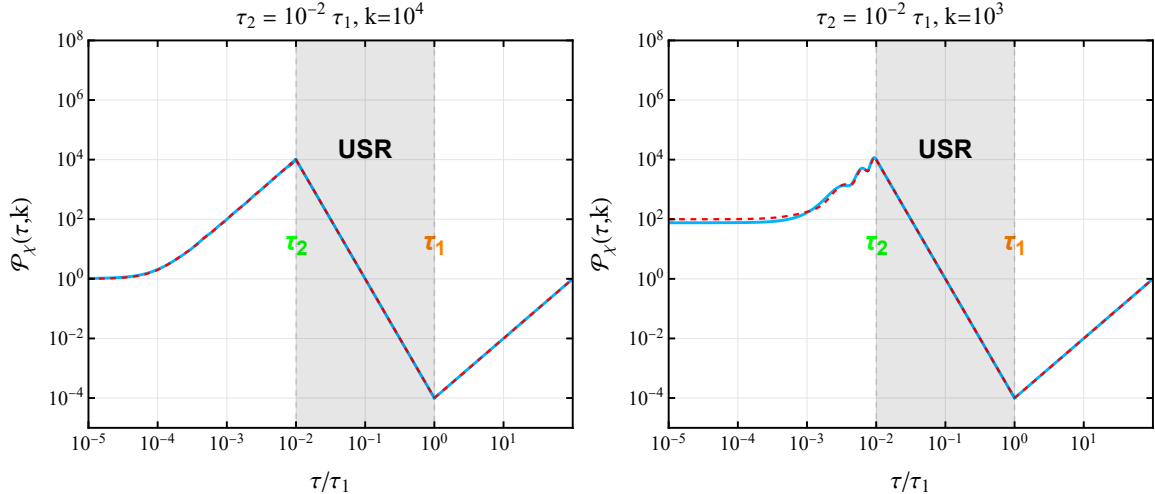


Figure 6: The time evolutions of power spectra across SR-USR-SR transitions in Case 3 for  $k = 10^3$  and  $k = 10^4$ , respectively. The blue solid curves refer to the exact solutions (4) with the coefficients (13), while the red dashed curves denote the asymptotic results given in Eqs. (54), (56) and (59). The parameters are chosen as  $\tau_2 = 10^{-2}\tau_1 = -0.01$ . All results are normalized by  $\mathcal{P}_\chi^{\text{USR}}(\tau_1, k)$  based on Eq. (4).

We introduce a enhancement factor to characterise the enhancement with respect to the vanilla superhorizon SR result (11),

$$\gamma \equiv \frac{\mathcal{P}_\chi^{\text{SR2}}(\tau_{\text{end}}, k)}{\mathcal{P}_{\chi, \text{CMB}}}. \quad (62)$$

Equation (61) yields

$$\gamma \simeq e^{6N_{\text{USR}}}, \quad (63)$$

which is consistent with the conventional results of USR inflation [71, 73, 74]. As expected, the longer USR duration leads to larger enhancement. The final value (61) is independent of  $k$ , this scale-invariant enhancement happens for all modes satisfying  $k \gg 1/(-\tau_2)$ . Because those modes are on superhorizon scales during the last phase. This fact is also evident in the numerical results, e.g., Fig. 2 in [73] and Fig. in Ref. [74].

### 3.3 Case 2

Now, we consider Case 2 of Fig. 1, such that  $-k\tau_2 < 1 < -k\tau_1$ , meaning the  $k$  mode exits the horizon during the intermediate USR phase. During the first SR phase, we can directly apply the subhorizon asymptotic power spectrum (54).

The evolution of a mode from subhorizon to superhorizon scales during the USR phase involves complexity, we therefore employ the exact result (29) to preserve accuracy. For  $-k\tau_1 > 1$ , we substitute Eq. (55) into Eq. (29) and obtain the leading-order asymptotics according to three Rules in Introduction,

$$\mathcal{P}_\chi^{\text{USR}}(\tau, k) \simeq \mathcal{P}_{\chi, \text{CMB}}(-\tau_1)^6 \left[ k^2(-\tau)^{-4} + \frac{6 \cos[2k(\tau - \tau_1)]}{-\tau_1}(-\tau)^{-5} + (-\tau)^{-6} \right], \quad (64)$$

which possesses three growing modes, scaling as  $(-\tau)^{-4}$ ,  $(-\tau)^{-5}$  and  $(-\tau)^{-6}$ . At the transition time  $\tau_1$ , we have  $(-\tau)^{-4} > (-\tau)^{-5} > (-\tau)^{-6}$  for  $\sqrt{6} < -k\tau_1 < \tau_1/\tau_2$ , while  $(-\tau)^{-5} > (-\tau)^{-4} > (-\tau)^{-6}$  for  $1 < -k\tau_1 < \sqrt{6}$ . If the ratio  $\tau_1/\tau_2$  does not exceed  $\sqrt{6}$ , only the former case applies.<sup>5</sup> Note that the  $(-\tau)^{-5}$  term is also oscillating in  $\tau$  on subhorizon scales ( $-k\tau > 1$ ), the oscillation frequency is proportional to  $k$  as shown in both panels of Fig. 7. In these two panels,  $\mathcal{P}_\chi^{\text{USR}}(\tau, k)$  first grows as  $(-\tau)^{-4}$  and oscillates, then switches to a  $(-\tau)^{-6}$  scaling near the horizon-crossing  $\tau_* = -1/k$ , marked by the black dotted vertical lines.

For the final SR phase, taking  $y < 1 < x$ , we obtain the following asymptotic expansions based on the coefficients in Eq. (13),

$$\lim_{-k\tau_2 < 1 < -k\tau_1} |A_3 - B_3|^2 \simeq \pi H^2 \frac{(-\tau_1)^6}{(-\tau_2)^6} \left[ 1 + 3 \frac{\sin(-2k\tau_1)}{(-k\tau_1)} \right], \quad (65a)$$

$$\lim_{-k\tau_2 < 1 < -k\tau_1} i(A_3^* B_3 - A_3 B_3^*) \simeq -\frac{3\pi H^2}{2} k^{-3} \frac{(-\tau_1)^6}{(-\tau_2)^9} \left[ 1 + 3 \frac{\sin(-2k\tau_1)}{(-k\tau_1)} \right], \quad (65b)$$

$$\lim_{-k\tau_2 < 1 < -k\tau_1} (A_3^* B_3 + A_3 B_3^*) \simeq \frac{9\pi H^2}{8} k^{-6} \frac{(-\tau_1)^6}{(-\tau_2)^{12}} \left[ 1 + 3 \frac{\sin(-2k\tau_1)}{(-k\tau_1)} \right]. \quad (65c)$$

Note that the term inside all square brackets,  $\left[ 1 + 3 \frac{\sin(-2k\tau_1)}{(-k\tau_1)} \right]$ , is a common factor in each coefficients.

<sup>6</sup> Specially, the leading oscillating piece  $\frac{\sin(-2k\tau_1)}{(-k\tau_1)}$  depends only on the variables  $-k\tau_1$ . Since the

<sup>5</sup> However, the asymptotic power spectrum (64) dose not yield a very robust approximation for  $1 < -k\tau_1 < \sqrt{6}$ , since  $-k\tau_1$  not sufficiently large compared to unity. In such a case, retaining more terms in the coefficients of Eq. (55) becomes necessary and no simple form is attainable.

<sup>6</sup> However, this factor can become negative within a narrow range of  $1.9 \lesssim -k\tau_1 \lesssim 2.6$ , which is problematic as it in principle cannot serve as the asymptotic form for an non-negative squared norm  $|A_3 - B_3|^2$ . This is because the asymptotic results (65) are not robust for small  $x$  and large  $y$  within the regime  $y < 1 < x$ . Despite this, it is found to be harmless for the subsequent discussions, and we are mainly interested in the regimes of  $x > 3$ .

mode is subhorizon at  $\tau_1$  (i.e.,  $x = -k\tau_1 > 1$ ), we keep the full oscillatory dependence on  $x$  in  $A_3$  and  $B_3$  (c.f., Eq. (36)). However, the condition  $y < 1$  allows us to apply a Taylor expansion of oscillatory terms in  $y$ , thereby eliminating all  $y$ -oscillations in Eq. (65).

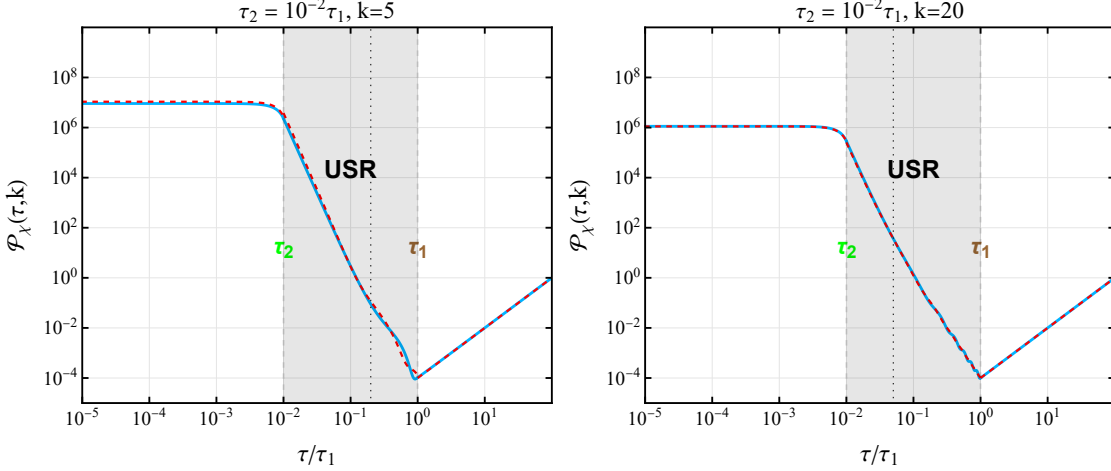


Figure 7: The evolutions of power spectra across SR-USR-SR transitions in Case 2 for  $k = 5$  and  $k = 20$ , respectively. The blue solid curve refers to the exact solution (4) with the coefficients (13), while the red dashed curve denotes the asymptotic expressions given in Eqs. (54), (64) and (66). The parameters are chosen as  $\tau_2 = 10^{-2}\tau_1 = -0.01$ .

Plugging those expressions in Eq. (65) into the superhorizon asymptotic expression (19), we yield

$$\lim_{-k\tau_2 < 1 < -k\tau_1} \mathcal{P}_\chi^{\text{SR2}}(\tau, k) \simeq \mathcal{P}_{\chi, \text{CMB}} e^{6N_{\text{USR}}} \left[ 1 + 3 \frac{\sin(-2k\tau_1)}{(-k\tau_1)} \right] \left[ 4 - 4 \frac{(-\tau)^3}{(-\tau_2)^3} + \frac{(-\tau)^6}{(-\tau_2)^6} \right]. \quad (66)$$

At the transition  $\tau_2$ , Eq. (66) gives

$$\lim_{-k\tau \ll 1} \mathcal{P}_\chi^{\text{SR2}}(\tau_2, k) \simeq \mathcal{P}_{\chi, \text{CMB}} e^{6N_{\text{USR}}}, \quad (67)$$

which is consistent with the result derived from Eq. (64) evaluated at  $\tau_2$ . We note that qualitatively similar time evolutions are also presented in Ref. [93] (cf. the right panel of Fig. 7 therein), which align with the behavior shown in our Figs. 4, 6, and 7.

According to Eq. (66), we estimate its value at the end of inflation as

$$\mathcal{P}_\chi^{\text{SR2}}(\tau_{\text{end}}, k) \simeq 4\mathcal{P}_{\chi, \text{CMB}} e^{6N_{\text{USR}}} \left[ 1 + 3 \frac{\sin(-2k\tau_1)}{(-k\tau_1)} \right], \quad (68)$$

which is plotted in Fig. 8 as a function of  $k/k_1$ . It exhibits an oscillation with an angular frequency  $-2\tau_1$ , which is also reported in Eqs. (2.12) and (6.5) of Ref. [83]. *Hence, wiggles in the final power spectrum reveals the information of the first transition time  $\tau_1$ .*

The enhancement factor defined in Eq. (62) for Eq. (68) is thus calculated as

$$\gamma \simeq 4e^{6N_{\text{USR}}} \left[ 1 + 3 \frac{\sin(-2k\tau_1)}{(-k\tau_1)} \right], \quad (69)$$

which exceeds the result for Case 3 given in Eq. (63). These oscillations gradually decay until some wavenumber smaller than  $k_2 = 1/(-\tau_2)$ , see Fig. 8. We estimate

$$\mathcal{P}_\chi^{\text{SR2}}(\tau_{\text{end}}, k \rightarrow k_2) \simeq 4\mathcal{P}_{\chi, \text{CMB}} e^{6N_{\text{USR}}}, \quad (70)$$

which agrees with Eq. (61) to within one order of magnitude.

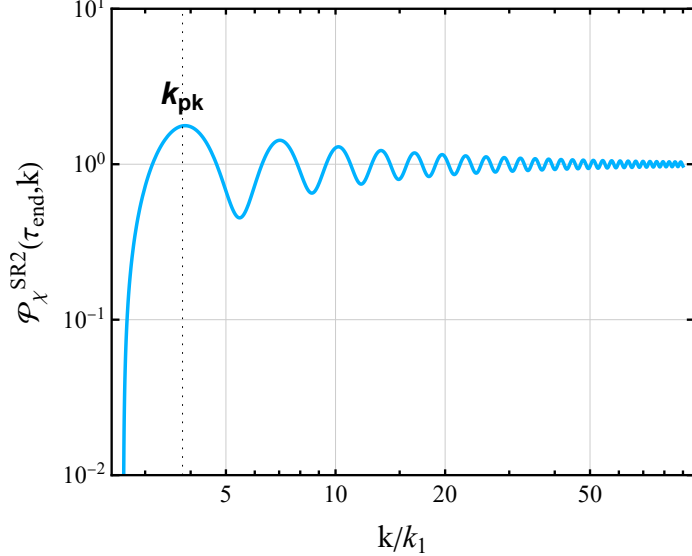


Figure 8: The final power spectrum  $\mathcal{P}_\chi^{\text{SR2}}(\tau_{\text{end}}, k)$  in Eq. (68). It exhibits an oscillation with an angular frequency  $-2\tau_1$  (c.f., Eq. (68)). The peak position  $k_{\text{pk}}$  of  $\mathcal{P}_\chi^{\text{SR2}}(\tau_{\text{end}}, k)$  is denoted by a black dashed vertical line. The value of  $\mathcal{P}_\chi^{\text{SR2}}(\tau_{\text{end}}, k)$  is normalized by  $\mathcal{P}_\chi^{\text{SR2}}(\tau_{\text{end}}, k \rightarrow k_2)$  given in Eq. (70).

Examining Eq. (69), the maximum enhancement happens around the lower bound  $-k_{\text{pk}}\tau_1 = 1$ , which determines the peak position,

$$k_{\text{pk}} \simeq 4k_1, \quad (71)$$

meaning  $k_{\text{pk}}$  exists the horizon soon after the first transition time  $\tau_1$ , which is consistent with previous literature (e.g., Refs. [73, 74, 83]). The peak value is correspondingly estimated as

$$\mathcal{P}_{\chi, \text{pk}} \equiv \mathcal{P}_\chi^{\text{SR2}}(\tau_{\text{end}}, k_{\text{pk}}) \simeq 7\mathcal{P}_{\chi, \text{CMB}} e^{6N_{\text{USR}}}, \quad (72)$$

which yields the enhancement factor,

$$\gamma_{\text{pk}} \simeq 7e^{6N_{\text{USR}}}, \quad (73)$$

which is approximately 7 times larger than the value given by Eq. (61), consistent with the numerical result of about 10 [74, 83].

## 4 Conclusion

In this work, we have revisited the behavior of linear curvature perturbations in an inflationary scenario consisting of successive slow-roll, ultra-slow-roll, and slow-roll phases with instantaneous transitions. By combining the junction condition method with carefully constructed asymptotic expansions of Hankel functions, and guided by three simple but powerful rules for identifying dominant contributions across transitions, we have derived accurate analytical expressions for the time evolution of the mode functions and the resulting power spectrum  $\mathcal{P}_R(\tau, k)$ .

Our analysis provides, for the first time, systematic asymptotic expressions of the linear power spectrum  $\mathcal{P}_R(\tau, k)$ , which capture the complete time evolution of the spectrum across all relevant  $k$  regimes. These analytical results successfully explain the key observational features of the USR-enhanced spectrum: the non-zero dip structure, the characteristic  $k^4$  growth, and the wiggles observed in the power spectrum at the end of inflation. These analytical expressions enhance the predictive power of the model, provide deeper physical insight into perturbation growth during USR phases, and establish a refined analytical basis for confronting future high-precision cosmological observations.

The methodology developed here, i.e., combining the junction method with careful asymptotic analysis of Hankel function solutions, offers a robust framework for studying non-attractor inflationary dynamics more broadly. Extending this approach to scenarios involving multiple or smooth transitions [77, 83], as well as incorporating non-perturbative effects across these transitions [82], promises to yield deeper insights into non-attractor inflationary dynamics and their phenomenological implications. We leave these important extensions to future work.

## A Consistent Check

Plugging Eq. (21) into Eq. (4), we derive the power spectrum in the SR phase as

$$\begin{aligned} \mathcal{P}_\chi^{\text{SR}}(\tau, k) &= \frac{|A|^2 + |B|^2}{\pi^3} [1 + k^2(-\tau)^2] \\ &+ \frac{AB^*}{\pi^3} e^{-2ik\tau} [-1 + 2ik(-\tau) + k^2(-\tau)^2] \\ &+ \frac{A^*B}{\pi^3} e^{2ik\tau} [-1 - 2ik(-\tau) + k^2(-\tau)^2], \end{aligned} \quad (74)$$

which is an exact expression obtained without resorting to any perturbative expansion. On superhorizon scales ( $-k\tau \ll 1$ ), the exponentials  $e^{-2ik\tau}$  and  $e^{2ik\tau}$  are both dominated by unity. Consequently, the leading asymptotic behavior is given by the constant mode,  $\lim_{-k\tau \ll 1} \mathcal{P}_\chi^{\text{SR}}(\tau, k) \simeq |A - B|^2/\pi^2$ . Keep terms up to order  $(-\tau)^6$ , we derive

$$\lim_{-k\tau \ll 1} \mathcal{P}_\chi^{\text{SR}}(\tau, k) \simeq \frac{|A - B|^2}{\pi^3} + \frac{2i(A^*B - AB^*)}{3\pi^3} k^3(-\tau)^3 + \frac{2(A^*B + AB^*)}{9\pi^3} k^6(-\tau)^6. \quad (75)$$

which coincides with Eq. (19).

For the intermediate USR phase, plugging Eq. (22) into Eq. (4) gives

$$\begin{aligned}\mathcal{P}_\chi^{\text{USR}}(\tau, k) = & \frac{|A|^2 + |B|^2}{\pi^3} \left[ (-\tau)^{-6} + k^2(-\tau)^{-4} \right] \\ & + \frac{AB^*}{\pi^3} e^{-2ik\tau} \left[ (-\tau)^{-6} - 2ik(-\tau)^{-5} - k^2(-\tau)^{-4} \right] \\ & + \frac{A^*B}{\pi^3} e^{2ik\tau} \left[ (-\tau)^{-6} + 2ik(-\tau)^{-5} - k^2(-\tau)^{-4} \right],\end{aligned}\quad (76)$$

which is an exact expression obtained without resorting to any perturbative expansion. On superhorizon scales ( $-k\tau \ll 1$ ), in order to retain all the growing modes, it is necessary to keep the higher-order terms in the expansions of  $e^{-2ik\tau}$  and  $e^{2ik\tau}$ . Thus, taking the leading terms in Eq. (76) gives the approximate expression

$$\begin{aligned}\lim_{-k\tau \ll 1} \mathcal{P}_\chi^{\text{USR}}(\tau, k) \simeq & -\frac{2(A^*B + AB^*)}{9\pi^3} k^6 + \frac{2(A^*B + AB^*)}{45\pi^3} k^8(-\tau)^2 \\ & + \frac{2i(AB^* - A^*B)}{3\pi^3} k^3(-\tau)^{-3} + \frac{|A + B|^2}{\pi^3} (-\tau)^{-6}.\end{aligned}\quad (77)$$

Comparison with Eq. (20), all growing modes and the constant mode agree as expected, but the decaying  $(-\tau)^2$  mode differs because higher-order terms in Hankel functions (18) were neglected.

## ACKNOWLEDGMENT

This work is supported by National Natural Science Foundation of China Grant (No.12503003), Jiangsu Basic Research Youth Project (No.BK20251001), Research and Practice Innovation Plan for Graduate Students in Jiangsu Province (No.KYCX25-4318), National Key R&D Program of China (Grant No.2021YFC2203100) and the National Natural Science Foundation of China (No.1243300). We thank Yudong Luo and Yu-Cheng Qiu for their contributions during the early stages of this work. C.C. thanks Diego Cruces and Xiao-Han Ma for their stimulating discussions and valuable feedback on the manuscript.

## References

- [1] Y. Akrami *et al.* (Planck), *Astron. Astrophys.* **641**, A10 (2020), arXiv:1807.06211 [astro-ph.CO]
- [2] A. Escrivà, F. Kuhnel, and Y. Tada, (2022), 10.1016/B978-0-32-395636-9.00012-8, arXiv:2211.05767 [astro-ph.CO].
- [3] A. M. Green and B. J. Kavanagh, *J. Phys. G* **48**, 043001 (2021), arXiv:2007.10722 [astro-ph.CO]
- [4] B. Carr and F. Kuhnel, *Ann. Rev. Nucl. Part. Sci.* **70**, 355 (2020), arXiv:2006.02838 [astro-ph.CO].

- [5] G. Domènech, *Universe* **7**, 398 (2021), arXiv:2109.01398 [gr-qc] .
- [6] O. Özsoy and G. Tasinato, *Universe* **9**, 203 (2023), arXiv:2301.03600 [astro-ph.CO] .
- [7] S. Pi, “Non-Gaussianities and Primordial Black Holes,” (2025) arXiv:2404.06151 [astro-ph.CO] .
- 
- [8] M. Biagetti, G. Franciolini, A. Kehagias, and A. Riotto, *JCAP* **07**, 032 (2018), arXiv:1804.07124 [astro-ph.CO] .
- [9] C. Pattison, V. Vennin, H. Assadullahi, and D. Wands, *JCAP* **08**, 048 (2018), arXiv:1806.09553 [astro-ph.CO] .
- [10] D. Cruces, C. Germani, and T. Prokopec, *JCAP* **03**, 048 (2019), arXiv:1807.09057 [gr-qc] .
- [11] H. Firouzjahi, A. Nassiri-Rad, and M. Noorbala, *JCAP* **01**, 040 (2019), arXiv:1811.02175 [hep-th] .
- [12] V. Atal, J. Garriga, and A. Marcos-Caballero, *JCAP* **09**, 073 (2019), arXiv:1905.13202 [astro-ph.CO] .
- [13] J. M. Ezquiaga, J. García-Bellido, and V. Vennin, *JCAP* **03**, 029 (2020), arXiv:1912.05399 [astro-ph.CO] .
- [14] D. G. Figueroa, S. Raatikainen, S. Rasanen, and E. Tomberg, *Phys. Rev. Lett.* **127**, 101302 (2021), arXiv:2012.06551 [astro-ph.CO] .
- [15] D. G. Figueroa, S. Raatikainen, S. Rasanen, and E. Tomberg, *JCAP* **05**, 027 (2022), arXiv:2111.07437 [astro-ph.CO] .
- [16] C. Pattison, V. Vennin, D. Wands, and H. Assadullahi, *JCAP* **04**, 080 (2021), arXiv:2101.05741 [astro-ph.CO] .
- [17] M. Biagetti, V. De Luca, G. Franciolini, A. Kehagias, and A. Riotto, *Phys. Lett. B* **820**, 136602 (2021), arXiv:2105.07810 [astro-ph.CO] .
- [18] M. W. Davies, P. Carrilho, and D. J. Mulryne, *JCAP* **06**, 019 (2022), arXiv:2110.08189 [astro-ph.CO] .
- [19] Y.-F. Cai, X.-H. Ma, M. Sasaki, D.-G. Wang, and Z. Zhou, *Phys. Lett. B* **834**, 137461 (2022), arXiv:2112.13836 [astro-ph.CO] .
- [20] Y.-F. Cai, X.-H. Ma, M. Sasaki, D.-G. Wang, and Z. Zhou, *JCAP* **12**, 034 (2022), arXiv:2207.11910 [astro-ph.CO] .
- [21] S. Pi and M. Sasaki, *Phys. Rev. Lett.* **131**, 011002 (2023), arXiv:2211.13932 [astro-ph.CO] .
- [22] S. Hooshangi, A. Talebian, M. H. Namjoo, and H. Firouzjahi, *Phys. Rev. D* **105**, 083525 (2022), arXiv:2201.07258 [astro-ph.CO] .

[23] N. Ahmadi, M. Noorbala, N. Feyzabadi, F. Eghbalpoor, and Z. Ahmadi, **JCAP** **08**, 078 (2022), arXiv:2207.10578 [gr-qc] .

[24] S. Hooshangi, M. H. Namjoo, and M. Noorbala, **JCAP** **09**, 023 (2023), arXiv:2305.19257 [astro-ph.CO] .

[25] S. Raatikainen, S. Räsänen, and E. Tomberg, **Phys. Rev. Lett.** **133**, 121403 (2024), arXiv:2312.12911 [astro-ph.CO] .

[26] E. Tomberg, **Phys. Rev. D** **108**, 043502 (2023), arXiv:2304.10903 [astro-ph.CO] .

[27] R. Inui, H. Motohashi, S. Pi, Y. Tada, and S. Yokoyama, **JCAP** **02**, 042 (2025), arXiv:2409.13500 [astro-ph.CO] .

[28] R. Inui, C. Joana, H. Motohashi, S. Pi, Y. Tada, and S. Yokoyama, **JCAP** **03**, 021 (2025), arXiv:2411.07647 [astro-ph.CO] .

[29] X. Wang, X.-H. Ma, and Y.-F. Cai, **Int. J. Mod. Phys. D** **34**, 2550027 (2025), arXiv:2412.19631 [astro-ph.CO] .

[30] A. Escrivà, J. Garriga, and S. Pi, (2025), arXiv:2512.04986 [astro-ph.CO] .

[31] A. Caravano, G. Franciolini, and S. Renaux-Petel, **Phys. Rev. D** **112**, 083508 (2025), arXiv:2506.11795 [astro-ph.CO] .

[32] H. Firouzjahi and A. Nassiri-Rad, **Phys. Rev. D** **112**, 123541 (2025), arXiv:2509.09608 [astro-ph.CO] .

[33] J. Kristiano and J. Yokoyama, **Phys. Rev. Lett.** **132**, 221003 (2024), arXiv:2211.03395 [hep-th] .

[34] S. Choudhury, M. R. Gangopadhyay, and M. Sami, **Eur. Phys. J. C** **84**, 884 (2024), arXiv:2301.10000 [astro-ph.CO] .

[35] J. Kristiano and J. Yokoyama, **Phys. Rev. D** **109**, 103541 (2024), arXiv:2303.00341 [hep-th] .

[36] A. Riotto, (2023), arXiv:2303.01727 [astro-ph.CO] .

[37] S. Choudhury, S. Panda, and M. Sami, **JCAP** **11**, 066 (2023), arXiv:2303.06066 [astro-ph.CO] .

[38] H. Firouzjahi, **JCAP** **10**, 006 (2023), arXiv:2303.12025 [astro-ph.CO] .

[39] H. Firouzjahi and A. Riotto, **JCAP** **02**, 021 (2024), arXiv:2304.07801 [astro-ph.CO] .

[40] H. Firouzjahi, **Phys. Rev. D** **108**, 043532 (2023), arXiv:2305.01527 [astro-ph.CO] .

[41] G. Franciolini, A. Iovino, Junior., M. Taoso, and A. Urbano, **Phys. Rev. D** **109**, 123550 (2024), arXiv:2305.03491 [astro-ph.CO] .

[42] S.-L. Cheng, D.-S. Lee, and K.-W. Ng, **JCAP** **03**, 008 (2024), arXiv:2305.16810 [astro-ph.CO] .

[43] J. Fumagalli, *JHEP* **05**, 162 (2025), arXiv:2305.19263 [astro-ph.CO] .

[44] J. Fumagalli, S. Bhattacharya, M. Peloso, S. Renaux-Petel, and L. T. Witkowski, *JCAP* **04**, 029 (2024), arXiv:2307.08358 [astro-ph.CO] .

[45] S. Maity, H. V. Ragavendra, S. K. Sethi, and L. Sriramkumar, *JCAP* **05**, 046 (2024), arXiv:2307.13636 [astro-ph.CO] .

[46] Y. Tada, T. Terada, and J. Tokuda, *JHEP* **01**, 105 (2024), arXiv:2308.04732 [hep-th] .

[47] H. Firouzjahi, *Phys. Rev. D* **109**, 043514 (2024), arXiv:2311.04080 [astro-ph.CO] .

[48] M. W. Davies, L. Iacconi, and D. J. Mulryne, *JCAP* **04**, 050 (2024), arXiv:2312.05694 [astro-ph.CO] .

[49] L. Iacconi, D. Mulryne, and D. Seery, *JCAP* **06**, 062 (2024), arXiv:2312.12424 [astro-ph.CO] .

[50] H. Firouzjahi, *Phys. Rev. D* **110**, 043519 (2024), arXiv:2403.03841 [astro-ph.CO] .

[51] K. Inomata, *Phys. Rev. Lett.* **133**, 141001 (2024), arXiv:2403.04682 [astro-ph.CO] .

[52] G. Ballesteros and J. Gambín Egea, *JCAP* **07**, 052 (2024), arXiv:2404.07196 [astro-ph.CO] .

[53] J. Fumagalli, *JHEP* **01**, 108 (2025), arXiv:2408.08296 [astro-ph.CO] .

[54] A. Caravano, G. Franciolini, and S. Renaux-Petel, *Phys. Rev. D* **111**, 063518 (2025), arXiv:2410.23942 [astro-ph.CO] .

[55] H. Firouzjahi, *Universe* **10**, 456 (2024), arXiv:2411.10253 [hep-ph] .

[56] K. Inomata, *Phys. Rev. D* **111**, 103504 (2025), arXiv:2502.08707 [astro-ph.CO] .

[57] C.-J. Fang, Z.-H. Lyu, C. Chen, and Z.-K. Guo, *Phys. Rev. D* **112**, 023547 (2025), arXiv:2502.09555 [gr-qc] .

[58] K. Inomata, *Phys. Rev. D* **111**, 123517 (2025), arXiv:2502.12112 [astro-ph.CO] .

[59] M. Braglia and L. Pinol, (2025), arXiv:2504.13136 [astro-ph.CO] .

[60] J. Kristiano and J. Yokoyama, (2025), arXiv:2504.18514 [hep-th] .

[61] Y. Ema, M. Hong, R. Jinno, and K. Mukaida, *JCAP* **01**, 040 (2026), arXiv:2506.15780 [astro-ph.CO] .

[62] C.-J. Fang, Z.-H. Lyu, C. Chen, and Z.-K. Guo, (2025), arXiv:2507.00077 [astro-ph.CO] .

[63] L. Iacconi, D. Mulryne, and D. Seery, (2026), arXiv:2601.14229 [astro-ph.CO] .

[64] N. C. Tsamis and R. P. Woodard, *Phys. Rev. D* **69**, 084005 (2004), arXiv:astro-ph/0307463 .

[65] W. H. Kinney, *Phys. Rev. D* **72**, 023515 (2005), arXiv:gr-qc/0503017 .

[66] M. H. Namjoo, H. Firouzjahi, and M. Sasaki, *EPL* **101**, 39001 (2013), arXiv:1210.3692 [astro-ph.CO] .

[67] J. Martin, H. Motohashi, and T. Suyama, *Phys. Rev. D* **87**, 023514 (2013), arXiv:1211.0083 [astro-ph.CO] .

[68] H. Motohashi, A. A. Starobinsky, and J. Yokoyama, *JCAP* **09**, 018 (2015), arXiv:1411.5021 [astro-ph.CO] .

[69] H. Motohashi, S. Mukohyama, and M. Oliosi, *JCAP* **03**, 002 (2020), arXiv:1910.13235 [gr-qc]

[70] H. Motohashi (2025) arXiv:2504.16757 [astro-ph.CO] .

[71] K. Dimopoulos, *Phys. Lett. B* **775**, 262 (2017), arXiv:1707.05644 [hep-ph] .

[72] C. Germani and T. Prokopec, *Phys. Dark Univ.* **18**, 6 (2017), arXiv:1706.04226 [astro-ph.CO] .

[73] C. T. Byrnes, P. S. Cole, and S. P. Patil, *JCAP* **06**, 028 (2019), arXiv:1811.11158 [astro-ph.CO]

[74] P. Carrilho, K. A. Malik, and D. J. Mulryne, *Phys. Rev. D* **100**, 103529 (2019), arXiv:1907.05237 [astro-ph.CO] .

[75] O. Ö兹soy and G. Tasinato, *JCAP* **04**, 048 (2020), arXiv:1912.01061 [astro-ph.CO] .

[76] G. Tasinato, *Phys. Rev. D* **103**, 023535 (2021), arXiv:2012.02518 [hep-th] .

[77] P. S. Cole, A. D. Gow, C. T. Byrnes, and S. P. Patil, *JCAP* **05**, 022 (2024), arXiv:2204.07573 [astro-ph.CO] .

[78] J.-X. Zhao and N. Li, *Eur. Phys. J. C* **84**, 222 (2024), arXiv:2403.01416 [astro-ph.CO] .

[79] J. Garcia-Bellido and E. Ruiz Morales, *Phys. Dark Univ.* **18**, 47 (2017), arXiv:1702.03901 [astro-ph.CO] .

[80] R. Zhai, H. Yu, and P. Wu, *Phys. Rev. D* **108**, 043529 (2023), arXiv:2308.09286 [gr-qc] .

[81] M. Cielo, G. Mangano, O. Pisanti, and D. Wands, *JCAP* **04**, 007 (2025), arXiv:2410.22154 [astro-ph.CO] .

[82] T. Fujita, R. Kawaguchi, M. Sasaki, and Y. Tada, *JCAP* **09**, 046 (2025), arXiv:2503.19744 [astro-ph.CO] .

[83] V. Briaud, A. Karam, N. Koivunen, E. Tomberg, H. Veermäe, and V. Vennin, *JCAP* **05**, 097 (2025), arXiv:2501.14681 [astro-ph.CO] .

[84] S. Pi and M. Sasaki, *Phys. Rev. D* **108**, L101301 (2023), arXiv:2112.12680 [astro-ph.CO] .

[85] D.-S. Meng, C. Yuan, and Q.-G. Huang, *Sci. China Phys. Mech. Astron.* **66**, 280411 (2023), arXiv:2212.03577 [astro-ph.CO] .

- [86] C. Chen, A. Ghoshal, Z. Lalak, Y. Luo, and A. Naskar, **JCAP** **08**, 041 (2023), arXiv:2305.12325 [astro-ph.CO] .
- [87] C. Fu and C. Chen, **JCAP** **05**, 005 (2023), arXiv:2211.11387 [astro-ph.CO] .
- [88] S. Pi and J. Wang, **JCAP** **06**, 018 (2023), arXiv:2209.14183 [astro-ph.CO] .
- [89] X. Wang, Y.-l. Zhang, and M. Sasaki, **JCAP** **07**, 076 (2024), arXiv:2404.02492 [astro-ph.CO] .
- [90] X. Wang, X.-H. Ma, and M. Sasaki, (2024), arXiv:2412.16463 [astro-ph.CO] .
- [91] N. Deruelle and V. F. Mukhanov, **Phys. Rev. D** **52**, 5549 (1995), arXiv:gr-qc/9503050 .
- [92] F. W. Olver, *NIST handbook of mathematical functions hardback and CD-ROM* (Cambridge university press, 2010).
- [93] G. Ballesteros, J. Rey, M. Taoso, and A. Urbano, **JCAP** **07**, 025 (2020), arXiv:2001.08220 [astro-ph.CO] .